Quaternary Science Reviews 330 (2024) 108595

Contents lists available at ScienceDirect

Quaternary Science Reviews

journal homepage: www.elsevier.com/locate/quascirev

Holocene changes in the position of the Southern Hemisphere Westerlies recorded by long-distance transport of pollen to the Kerguelen Islands

Maaike Zwier [a,*], Willem G.M. van der Bilt [b], Tobias Schneider [c,d], William J. D'Andrea [c], Jostein Bakke [b], Nathalie Van der Putten [e], Anne E. Bjune [a]

[a] Department of Biological Sciences and Bjerknes Centre for Climate Research, University of Bergen, Thormøhlensgate 53A/B, 5006, Bergen, Norway
[b] Department of Earth Science and Bjerknes Centre for Climate Research, University of Bergen, Allégaten 41, 5007, Bergen, Norway
[c] Lamont-Doherty Earth Observatory, Columbia University, Palisades, NY 10964, USA
[d] Department of Surface Waters–Research and Management, Swiss Federal Institute of Aquatic Sciences and Technology (EAWAG), Dübendorf, Switzerland
[e] Department of Earth Sciences, Vrije Universiteit Amsterdam, De Boelelaan 1085, 1081, HV, Amsterdam, Netherlands

ARTICLE INFO

Handling Editor: Yan Zhao

Keywords:
Southern Hemisphere westerly winds
Palynology
Vegetation dynamics
Sedimentology
Sub-Antarctic
South Africa
Paleoclimatology
Holocene

ABSTRACT

The Southern Hemisphere Westerlies (SHW) are a vital part of the Southern Hemisphere's coupled ocean-atmosphere system and play an important role in the global climate system. The SHW affect the upwelling of carbon-rich deep water and exchange of CO_2 from the ocean to the atmosphere by driving the Antarctic Circumpolar Current. On seasonal to millennial timescales, changes in the strength and position of the SHW are associated with temperature and precipitation changes throughout the extratropical Southern Hemisphere. Understanding the behaviour of the SHW under different background climate states is important for anticipating its future behaviour and remains a subject of ongoing research. Terrestrial paleoclimate records from lake sediments are valuable for reconstructing past atmospheric change and records from the handful of sub-Antarctic islands provide the opportunity to develop datasets to document spatio-temporal patterns of long-term SHW behaviour. Here, we generate palynological, microcharcoal, and sedimentological reconstructions (including CT imagery, μXRF analysis, magnetic susceptibility, and loss-on-ignition) on lake sediments from the Kerguelen Islands (49°S) to constrain variability in Holocene vegetation, climate, and atmospheric circulation (SHW position). Due to the influence of the SHW on the Kerguelen Islands, the influx of long-distance transported (LDT) pollen and microcharcoal from southern Africa serve as proxies for the meridional position of the SHW. In contrast with the stable conditions that prevailed on the Kerguelen Islands over the past 8,600 cal yr BP, our findings reveal a highly dynamic Early Holocene period. Consistent with local palynological evidence of warmer conditions, a high influx of LDT pollen and charcoal from southern Africa suggest that the SHW core belt was located further south of the Kerguelen Islands during this time. Comparison against paleoclimate records from the surrounding region and beyond suggests that the inferred changes might be explained by changes to our planet's interhemispheric thermal gradient, triggered by North Atlantic cooling in response to melting of the last remnants of the Laurentide Ice Sheet.

1. Introduction

The Southern Hemisphere Westerly Winds (SHW) are the main atmospheric feature of the extratropical Southern Hemisphere (SH), and exert important feedbacks on regional and global climate through its effects on 1) temperature gradients (Fogt and Marshall, 2020; Frölicher et al., 2015), 2) precipitation distribution (Fletcher and Moreno, 2011; Mayr et al., 2007), 3) the position and intensity of high latitude storm tracks (Yin, 2005), 4) global ocean circulation, including the Atlantic meridional overturning circulation (Hall and Visbeck, 2002; Toggweiler et al., 2006), 5) oceanic uptake of carbon and heat (Gottschalk et al., 2020; Landschützer et al., 2015), and 6) Antarctic sea-ice extent (Hall and Visbeck, 2002; Purich et al., 2016).

These components and processes are fundamentally linked to changes in the position of the SHW core belt (the latitudes where zonal winds are strongest), which is currently located at approximately 52°S (Swart and Fyfe, 2012). For example, a more southern position of the SHW enhances upwelling and outgassing of CO_2 from the ocean to the

* Corresponding author.
E-mail address: maaike.zwier@uib.no (M. Zwier).

https://doi.org/10.1016/j.quascirev.2024.108595
Received 5 September 2023; Received in revised form 16 February 2024; Accepted 29 February 2024
Available online 8 March 2024

atmosphere, affecting the Southern Ocean carbon storage (Anderson et al., 2009; Hodgson and Sime, 2010; Toggweiler et al., 2006). Over the instrumental period, changes in the SHW are associated with the Southern Annular Mode (SAM): changes in the pressure gradient between 40 and 65°S that represent the leading mode of atmospheric variability in the extratropical Southern Hemisphere (Thompson and Wallace, 2000). Coupled SHW-SAM variability alternates between two extremes: a northward expansion of the core belt that is accompanied by weaker winds (negative SAM), and a southward shift that is associated with stronger winds (positive SAM) (Fogt and Marshall, 2020). These changes occur across a range of different timescales, from 1) the seasonal cycle as the SHW's core belt moves southward in the austral summer and northwards during the austral winter, to 2) millennial timescales, as a result of changes in insolation or ocean circulation (Lamy et al., 2010). Because of the global climate feedbacks related to changes in the SHW, and in light of rapid on-going changes in response to anthropogenic warming (Abram et al., 2014), it is important to understand past movements of the SHW to better anticipate their future evolution (IPCC, 2023).

In the absence of long observational timeseries, paleoclimate data can help us better understand the causes and consequences of these globally relevant SHW-climate interactions (Hodgson and Sime, 2010). Terrestrial records are essential for reconstructing atmospheric conditions, but landmasses are scarce in the Southern Ocean. Most SHW reconstructions come from Patagonia (e.g Kilian and Lamy, 2012; Kohfeld et al., 2013; Moreno et al., 2021, 2010; Reynhout et al., 2019) and paleoclimate data from sub-Antarctic islands are important to provide greater spatial coverage (e.g. Perren et al., 2020; Saunders et al., 2018, 2015; van der Bilt et al., 2022; Van der Putten et al., 2015; Zwier et al., 2022).

Reconstructing past wind conditions is challenging, and often inferred through indirect proxies that record SHW-driven precipitation and temperature changes (Lamy et al., 2010). The analysis of wind-blown particles, e.g. dust, pollen, and microcharcoal, provides a more direct way of reconstructing variations in atmospheric circulation (Saunders et al., 2018; Turney et al., 2016). These microscopic particles can be transported over very long distances and are therefore useful in the sub-Antarctic (Neff and Bertler, 2015). Pollen grains provide particular value, because identification to species can allow identification of the source region (Jessen et al., 2011; Rodrigues et al., 2023). Deposition sites downwind from source areas of long-distance transported (LDT) particles provide the opportunity to reconstruct changes in wind strength and position (Strother et al., 2015; Turney et al., 2016; Zwier et al., 2022).

The Kerguelen Islands (49°S) are ideally located to capture LDT particles from southern Africa (33°S) due to the cyclonic nature of SHW storm tracks that transport air in a south-easterly direction (Neff and Bertler, 2015; Reijmer et al., 2002). LDT particles from southern South America, located >9,000 km upwind of, and at similar latitude to, the Kerguelen Islands could potentially also reach the island (Neff and Bertler, 2015). Previous palynological work focused on local vegetation reconstructions identified LDT pollen on the Kerguelen Islands (Bellair, 1970; Young and Schofield, 1973); another study examined LDT pollen on the island between 16,000 and 11,000 cal yr BP (Van der Putten et al., 2015).

Here, we provide a multiproxy, high-resolution Holocene lake sediment record from the western Kerguelen Islands to reconstruct zonal SHW changes. Palynological and sedimentological analyses were carried out to **1**) reconstruct Holocene vegetation and climate changes on the Kerguelen Islands, **2**) identify Holocene SHW wind variability over the Southern Indian Ocean, and **3**) identify possible links to drivers of SHW-climate change.

1.1. Study area

The French Kerguelen Islands (49°S, 69°E) are situated in the South Indian Ocean, approximately 4000 km southeast of the nearest landmass – southern Africa (Fig. 1a). The islands are of volcanic origin and mostly covered by flood basalts (Gautier et al., 1990). The western part of the Kerguelen Islands is mountainous – most peaks reach over 1000 m above sea level – and is partly covered by the rapidly retreating Cook Ice Cap (Charton et al., 2022; Verfaillie et al., 2021).

Climate on the Kerguelen Islands is characterized by moderate seasonal temperature fluctuations with mean temperatures between 1989 and 2019 of 7.8 °C in summer and 2.5 °C in winter (Trouet and Van Oldenborgh, 2013). Annual precipitation averages <800 mm around the Port-aux-Français meteorological station on the eastern (down-wind) side of the Kerguelen Islands (Fig. 1b) and can reach >3200 mm on the western side (up-wind) near our study site (Frenot et al., 1997). The mean wind velocity is about 10 m/s and is higher during winter (Pendlebury and Barnes-Keoghan, 2007; Van der Putten et al., 2015).

1.1.1. Setting

Our study site, the informally named Lake 5 (49.14°S, 69.09°E), is located on the north-western side of the largest island of the Kerguelen Islands (Fig. 1b). The lake's position ~130 m above sea level and 8 km to the north of the Cook Ice Cap (Fig. 1b) has sheltered it from glacial runoff. The basin measures ~0.2 km^2 and has a maximum depth of ~24 m (Fig. 1d). There are four small gullies draining into the lake and there is one outlet to the north (Fig. 1c). The relatively small catchment of Lake 5 measures ~1,3 km^2 and is partly vegetated, only the exposed higher ridges are completely bare (Fig. 1c). The rocky hillsides are dominated by *Azorella selago* cushions. The more sheltered slopes (mostly facing east) are dominated by grasses. *Acaena magellanica, Colobanthus* spp., *Pringlea antiscorbutica, Lycopodium* spp. as well as various mosses and lichen are recorded in the lake's wider surroundings. *Ranunculus* spp. is predominantly growing partly submerged around the stream edges.

2. Material and methods

2.1. Fieldwork

In the austral summer of 2019/2020, a field campaign was undertaken to Lake 5 (Fig. 1). After surveying lake bathymetry using a Lowrance echo sounder and compiling a map on-site, six profiles with ground penetrating radar (50 MHz unshielded antennas inside 110 mm PVC tubes) were collected to map out the sediment distribution in the deepest parts of the lake. Based on this, three cores were retrieved from the depocenters of the two sub-basins in the lake (Fig. 1d) with a modified Nesje piston corer (Nesje, 1992). Additional gravity cores were obtained at the same locations to capture surface sediments. Representative plant samples were collected from the surrounding area (Fig. 1c) to help build a pollen and spore reference collection. The sediment cores were stored in dark and cold (4 °C) conditions at the EARTHLAB, Bergen, Norway, before splitting and logging. Here we report results from the composite (piston + gravity) sediment core L5-03-19, recovered in the northern sub-basin (Fig. 1d), which contains the longest continuous laminated (undisturbed) record with few inverted ages (section 3.1 and 3.2).

2.2. Lithology and geochemical analysis

Prior to destructive analysis, the core sections were scanned using a Cox Analytical ITRAX X-Ray Fluorescence (XRF) core scanner, to acquire downcore semi-quantitative elemental profiles (Croudace et al., 2006). The sections were logged at 500 μm resolution using a Molybdenum (Mo) tube (30 kV, 27 mA) and a dwell time of 10s to better measure heavier elements. For further analysis, we excluded individual elemental profiles with a mean square error (MSE) > 2 and total kilo counts per second (kcps) outside the 20 to 35 range, and omitted elements with an autocorrelation <0.7 at a 2.5 mm lag to remove noisy

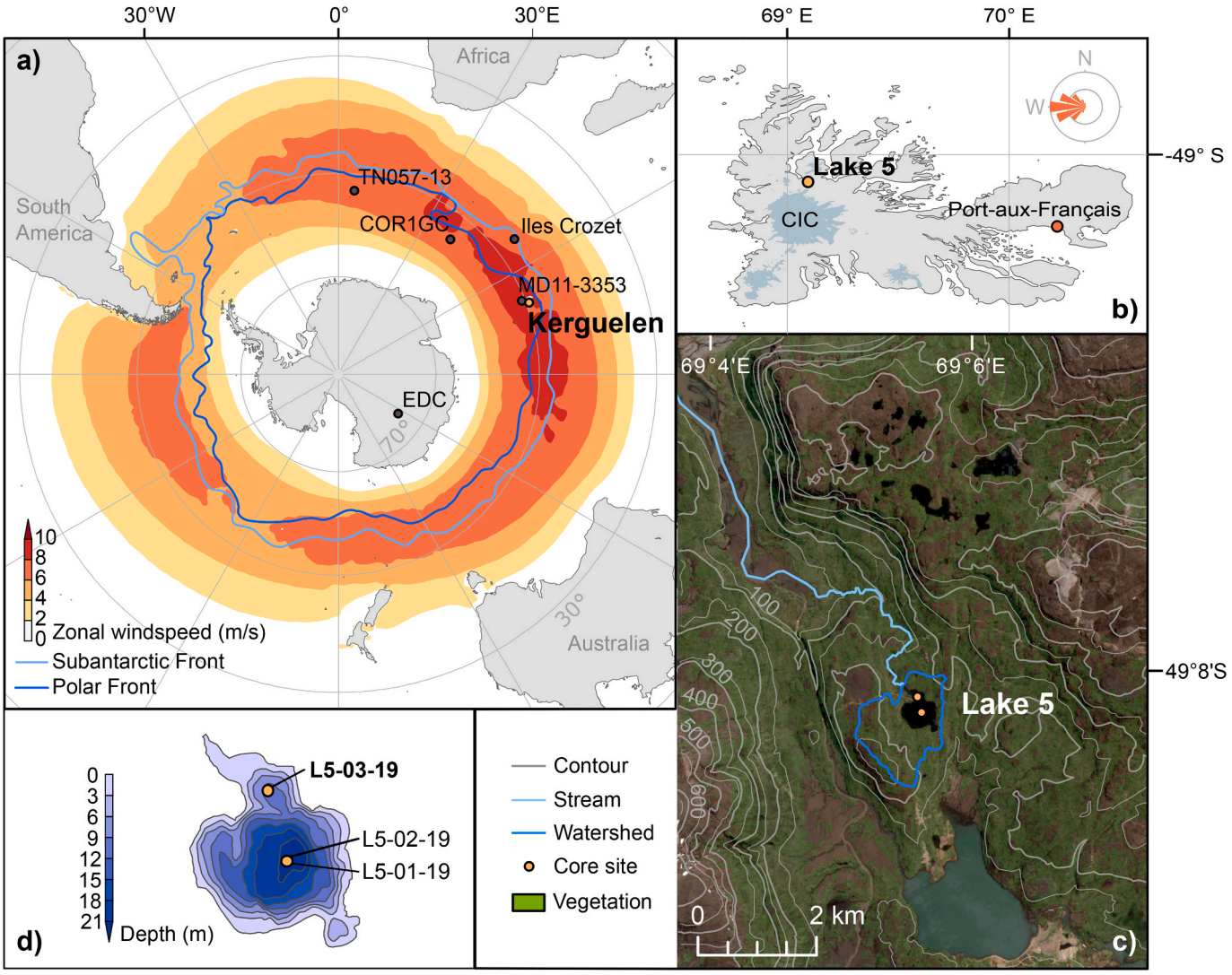

Fig. 1. a) Overview map showing the modern position of the main atmospheric and oceanic circulation systems around Antarctica. The Southern Hemisphere Westerly Winds are indicated by the average zonal windspeed at 10m height from 1950 to 2021, as calculated from ERA5 reanalysis data (Hersbach et al., 2020). **b)** Inset of the Kerguelen Islands showing Lake 5, the nearest meteorological station at Port-aux-Français, recorded wind direction over the last 30 years after Meteoblue (2023), and the Cook Ice Cap (CIC). **c)** Lake 5 site topography, catchment area, and outlet. The vegetation cover is shown by the normalized different vegetation index (NDVI) calculated from Copernicus Sentinel-2 data acquired on 2021-11-30 (EO Browser). **d)** Bathymetric map of Lake 5 (section 2.1); orange circles indicate coring sites.

data, following the recommendations of Bishop (2022). Counts were normalized against the sum of incoherent and coherent currents (inc + coh) to account for downcore variability in water content and organic matter (Kylander et al., 2012). To identify internal sedimentary structures, the cores were scanned using a ProCon-X-Ray CT-ALPHA Computed Tomography (CT) scanner set at 135 kV and 900 μA, with a 0.5 mm Cu filter, an exposure time of 334 ms, and using 2400 rotations per projection. CT imagery was visualized and analysed with the ThermoFisher Avizo software (version 9), generating down-core greyscale values at 5 mm resolution using the spline probe tool. To help identify changes in mineral magnetic content and grain size, magnetic susceptibility (MS) was measured using a Bartington Instruments MS2G loop sensor mounted on a Geotek core scanner at 0.5 cm resolution (Sandgren and Snowball, 2002).

Following core scanning, the gravity and piston core sections were aligned using their respective Zirconium (Zr) stratigraphy, and our composite depth scale was created using QAnalySeries 1.5.1 (Kotov and Paelike, 2018). Thereafter, we carried out destructive physical analyses. Loss-on-ignition (LOI) and dry-bulk density (DBD) were acquired from 1 cm^3 samples taken at ~4 cm intervals throughout the core. For this purpose, samples were dried at 105 °C overnight and subsequently burned at 550 °C for 6 h after Heiri et al. (2001).

Following acquisition and processing, principal component analysis (PCA) was performed on square-root transformed multi-proxy data using base R (R Core Team, 2022) to identify gradients of change. In addition, unconstrained cluster analysis was performed with the rioja package (Juggins, 2015) to help distinguish different sedimentological facies.

2.3. Chronology

A total of 24 samples for ^{210}Pb dating and 11 samples for ^{137}Cs dating from the top 12 cm of the gravity core were measured at NIOZ dating facility in the Netherlands (Supplementary Fig. 1). Moreover, fifteen terrestrial plant macrofossil samples (Table 1), wet-sieved through a 125 μm mesh and dried, were measured for radiocarbon dating at either the Poznań Radiocarbon Laboratory, Poland (Poz-samples) (Goslar et al., 2004), or Lund Radiocarbon Dating Laboratory, Sweden

Table 1
Radiocarbon dates obtained for terrestrial macrofossil (moss) samples from core L5-03-19. Showing the Lab ID, sample mid-depth, sample weight, the ^{14}C age, 1σ error, the resulting bacon model age, and the calibrated ages (SHCal20; Mean, Min, Max), and the explained probability.

Lab ID	Mid depth (cm)	Weight (mgC)	Age (^{14}C yr)	Error (±1σ)	Model (cal yr BP)	Mean (cal yr BP)	Min (cal yr BP)	Max (cal yr BP)	Probability (%)
Poz-139136	27.22	NA	1620	30	1432	1454.5	1368	1541	93.3
Poz-143957	46.72	NA	2565	35	2570	2588	2423	2753	93.6
Poz-139137	63.22	0.3	3655	30	3870	3957.5	3824	4091	91.1
Poz-143958	82.72	0.8	4640	35	5270	5260	5040	5480	90.5
Poz-139213	110.72	0.4	6690	40	7486	7522.5	7430	7615	92.7
Poz-143930	124.72	NA	6910	40	7758	7712.5	7585	7840	94.1
Poz-143960	142.22	NA	7460	40	8206	8267.5	8165	8370	85.5
LuS 17769	147.72	0.8	7815	45	8521	8585	8400	8770	93.9
Poz-138826	187.22	1.0	8110	50	8677	8920	8695	9145	85.9
Poz-143932	210.72	NA	9670	50	NA	10973	10750	11195	94.7
Poz-138827	226.22	NA	10520	60	NA	12388	12085	12690	94.3
Poz-143931	255.72	NA	8050	50	9330	8832.5	8635	9030	91.1
LuS 16762	262.22	NA	8450	45	9465	9397.5	9255	9540	93.1
LuS 16763	295.22	1.3	9090	45	10058	10270	10110	10430	80.8
LuS 16764	343.22	1.2	9665	45	10991	10972.5	10755	11190	94.9

(LuS-samples).

2.4. Palynological and microcharcoal analysis

A pollen and spore reference collection was constructed using modern plant samples collected during fieldwork to the Kerguelen Islands in 2006, 2019–2020, and nearby Possession Island (Iles Crozet) – which has a similar flora to the Kerguelen Island (Van der Putten et al., 2008, 2015) – in 1999 (Fig. 1a and c). Pollen from the plant samples were treated with KOH, sieved, acetolysed, and mounted in glycerol gelatine. Sediment samples (1 cm^3) taken at 4 cm intervals throughout the Lake 5 record, were sieved and treated with KOH, HF, and acetolysis according to Faegri and Iversen (1989). A known quantity of *Lycopodium clavatum* spores (batch nr. 100320201, produced at Lund University, Sweden) were added before treatment to allow calculation of concentrations. The residue was stored in glycerol and mounted on microscope slides. Identification and counting of pollen, spores, non-pollen palynomorphs (NPP's), and microcharcoal was carried out with a Zeiss light microscope at 400x magnification, using the constructed pollen reference collection at the University of Bergen, Norway, works of Barrow (1976), Reille (1992), Scott (1982), Van Zinderen Bakker (1956a, 1956b), Van Zinderen Bakker and Coetzee (1959) and the online pollen reference collection for the Cape Floristic Region (Nelson Mandela University, 2019). Exotic pollen taxa were categorized into different parent plant source regions (Chevalier et al., 2021; Quick et al., 2016; Zhao et al., 2016) (Supplementary Table 4). Preservation status of the pollen was noted according to the classification by Mansilla et al. (2018) to make inferences of mechanical (broken or crumpled grains) and biochemical (corroded or degraded grains) deterioration processes in the catchment. All native phanerogam taxa were included in the pollen sum (Greene and Greene, 1963; Supplementary Table 3). Provided sufficient pollen concentration, samples were counted to a pollen sum of >300 grains. Samples with pollen sum <100 were discarded. Pollen diagrams were constructed using Tilia 2.6.1 (Grimm, 1992). Constrained cluster analysis (CONISS, Grimm, 1987) of the taxa included in the pollen sum was performed using the vegan package in R (Oksanen et al., 2020). The number of interpretable clusters was determined with a broken stick model using the rioja package (Juggins, 2015).

3. Results

3.1. Lithology

The alignment of the gravity core to the piston core resulted in a combined 357.5 cm long record (Supplementary Fig. 2). Visual logging and geochemical analysis of the record (section 2.2) revealed three main sediment facies: organic-rich laminated mud; inorganic laminated sand; and (coarse) sand and gravel (Fig. 2).

The bulk of the sediment record consist of brown organic-rich cm-scale laminated mud (Fig. 2). This facies is characterized by high LOI, inc/coh, and Br values – which are all widely used measures of organic content (Davies et al., 2015; Kylander et al., 2012) – and low CT greyscale values – indicative for low sediment density (Fig. 2). CT imagery reveals small pebbles embedded in the mud (Supplementary Fig. 3). From 349.2 to 232.5 the pebbles are rare, from 232.5 to 185 cm depth they are abundant, and from 185 to 0 cm they are frequent. CT imagery also reveals three intervals with folded (F) laminae from 282 to 294 cm (F1), 299–304 cm (F2), and 320–323 cm (F3) depth (Supplementary Fig. 3).

At several intervals at the base of the record, the sediment consists of laminated grey to brown inorganic fine-grained sand containing a few small pebbles: from 357.5 to 349.2 cm, 329 to 323 cm, 274.5–275.5 cm, and 232.5 to 230 cm (beige layers in Fig. 2). High values of CT greyscale, MS, and Ti – indicative for minerogenic content (Davies et al., 2015) – correspond with low values of LOI, inc/coh, and Br.

The laminated sediment is interspersed by four thick coarse sand and gravel layers with a sharp and undulating base from 118 to 124.5 cm (E1), 131–141.5 cm (E2), 150–185 cm (E3), and 232.5–255 cm (E4), and ten mm-thick (coarse) sand layers (grey layers in Fig. 2, Supplementary Fig. 3). Visual inspection (smear slides) of the layers revealed the presence of tephra shards (Supplementary Fig. 4). This facies is characterized by low MS and Ti values and high K and Zr values – which may be linked to an increase in grain size (Davies et al., 2015). These characteristics distinguish this facies from the inorganic laminated sand. We

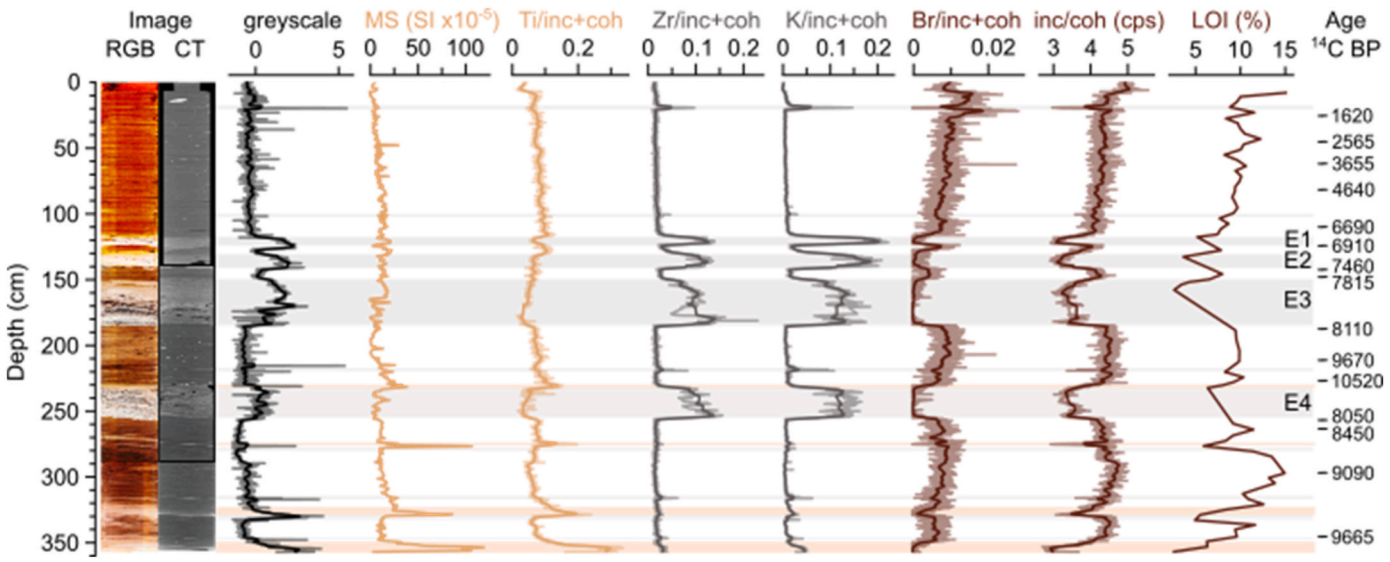

Fig. 2. Summary of sedimentological data from Lake 5 on a depth scale. Showing from left to right: enhanced colour (RGB) and CT imagery, greyscale values, magnetic susceptibility (MS), a selection of the geochemical (μXRF) variables, loss-on-ignition (LOI), and ^{14}C sample ages in yr BP. The μm-scale XRF and CT greyscale (section 2.2) records show a 25 mm running mean to improve readability and enhance comparability with the mm-scale resolution MS and LOI records. Inorganic laminated sand layers are shown in beige. Coarse sand and gravel layers are shown in grey, including the event layers E1-E4.

argue that this facies represents abruptly deposited event (E) layers and discuss how this influences the age-depth model in section 3.2.

Principal component analysis (PCA) conducted on the μXRF data from Lake 5 shows three distinct groups corresponding to the three sediment facies of our record (Fig. 3). The inorganic laminated sand is represented by group 1 and is associated with high counts of the elements Ti, Ca, Fe, Ni, Cu, Sr, Cr, and V. The (coarse) sand and gravel is represented by group 2 and is associated with high counts of Zr, K, Rb, Zn, and Y. The organic laminated mud is associated with group 3 and includes high counts of Br.

3.2. Age-depth model

Our ^{210}Pb profile was excluded because of visual signs of sediment homogenization in the top 4.5 cm as revealed by CT imagery and the ^{210}Pb inventory (Supplementary Fig. 1). However, the ^{137}Cs activity showed two peaks in the top 2 cm, which followed the atmospheric fallout pattern expected for this latitude (Arnaud et al., 2006). They were identified as 1952 and 1963 AD (Supplementary Fig. 1) and used to further constrain the age-depth model (Fig. 4). Radiocarbon dates (Table 1) were calibrated using the SHCal20 calibration curve (Hogg et al., 2020) and are presented as calibrated years before present (cal. yr BP), with present being 1950 AD. Radiocarbon dates Poz-143932 and Poz-138827 were excluded from the age-depth model due to their inverted ages. The sediment interval where these samples were taken showed many coarse-grained particles – indicating a high-energy environment – supporting the notion that these old ages might derive from reworked material from the surrounding slopes (Fig. 2). Based on the presence of sharp and undulating contacts with underlying sediments (Supplementary Fig. 3), the presence of tephra shards (Supplementary Fig. 4), and temporal proximity of the radiocarbon dates LuS17769, Poz-138826, and Poz-143931 (Table 1), we interpret the coarsely

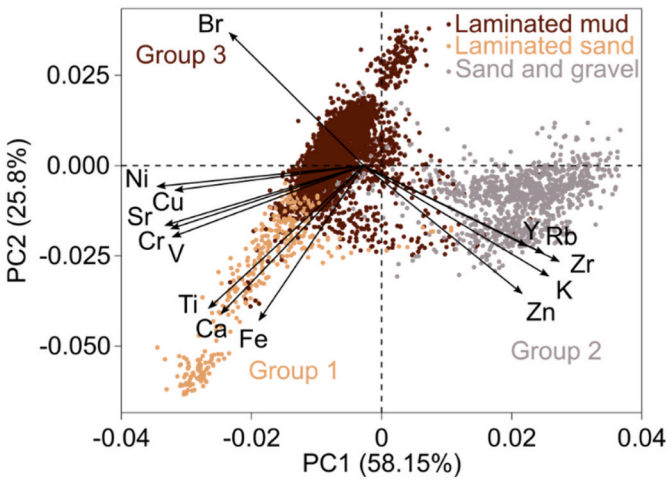

Fig. 3. Principal component analysis (PCA) of the selected geochemical (XRF) data from Lake 5 (section 2.2). The percentage of variance explained by principal component (PC) 1 and 2 are displayed on the axes. Colour coding corresponds to Fig. 2.

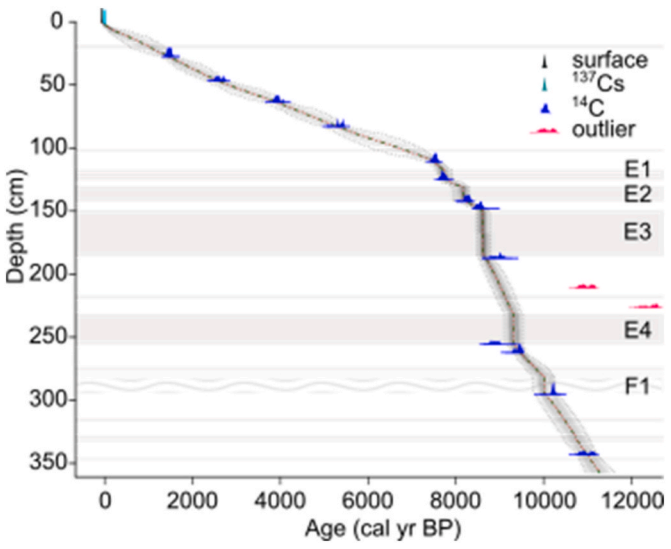

Fig. 4. Age-depth model for the composite sediment record L5-03-19. The grey layers represent layers of instant deposition that were treated as slumps in the age-depth model, E1-E4 mark the thick event layers, and F1 the overturned folded interval.

grained sand and gravel layers as slumps (Supplementary Table 2). In addition, CT imagery reveals the presence of overturned folds and torn sediments in the interval between 282 and 294 cm depth (layer F1, Supplementary Fig. 3). Based on these signs of disturbance, we also treated this layer as a slump. CT imagery from folded layers F2 and F3 did not reveal overturned folds and did therefore not require treatment as slumps. The final chronology (Fig. 4) was generated using a Bayesian age-depth model using the *rbacon* v2.5.8, with standard settings and a section thickness of 4 cm (Supplementary Table 1, Blaauw et al., 2022). In the Early Holocene, the sediment accumulation rate averages 0.54 mm/yr and decreases to 0.17 mm/yr after ca. 8,600 cal yr BP (Fig. 4).

3.3. Palynological analysis

The native pollen spectrum (Fig. 5) is dominated by pollen from *Azorella selago*, Poaceae, *Acaena magellanica*, and *Carex austrocompacta* – formerly named *Uncinia compacta* (Waterway et al., 2015). Pollen and spores from less-abundant native vascular plants, mosses, and fungi on average only make up 4% of the pollen sum (Supplementary Fig. 6). The LDT pollen is dominated by southern African Fynbos, Succulent Karoo, and cosmopolitan taxa (Fig. 5), on average LDT pollen make up 6% of the pollen sum, with peaks up to 22% in the Early Holocene (Supplementary Fig. 6a). Microcharcoal in the pollen slides ranges from 10 to 100 μm in length on the longest axis. The structure of charred cell fragments and bilobate phytoliths reveal the presence of grass-type charcoal (Yost et al., 2018; Supplementary Fig. 5). The influx of microcharcoal is positively correlated to the influx of LDT pollen ($r = 0.6$, $p \ll 0.001$). Based on the cluster analysis of all native phanerogam taxa, the pollen diagram is subdivided into two sub-zones.

Zone 1 (~11,300–7,400 cal yr BP) is dominated by varying abundance of pollen from Poaceae, anti-phased to variations in *Acaena magellanica,* and *Carex austrocompacta*, and green algae colonies (Fig. 5). After three of the inorganic laminated sandy layers (Figs. 2 and 5, beige layers), *Acaena magellanica* pollen abundance shortly peaks from ~10% to 40–50%, coincident with a decline in Poaceae pollen from ~60% to 20% (Fig. 5). Cryptogam spores show a high species diversity and abundance throughout zone 1 (Supplementary Fig. 6). From ~8,600 cal yr BP, pollen from *Azorella selago* increases in abundance and it remains the dominant taxon for the remaining part of zone 1. Pollen preservation is generally good, while poorly preserved pollen grains are mostly crumpled (Supplementary Fig. 6a). Algal colonies from *Botryococcus* and *Pediastrum*, show high but varying abundance reaching peaks of 260% and 600% (calculated relative to the pollen sum) respectively. LDT pollen influx is high (~50 pollen $cm^{-2}yr^{-1}$) with peaks to 100 pollen $cm^{-2}yr^{-1}$ coinciding with the peaks in *Azorella selago,* and is dominated by pollen from Fynbos, Karoo, and cosmopolitan taxa (mainly Asteraceae – dominated by *Artemisia* and *Pentzia*-type, Aizoaceae, and Ericaceae) (Fig. 5, Supplementary Fig. 6). Microcharcoal fragments show a high influx (~60 grains $cm^{-2}yr^{-1}$) with peaks reaching 150 grains $cm^{-2}yr^{-1}$, coincident with the LDT pollen maxima until 8,600 cal yr BP.

Zone 2 (~7,400 to −69 cal yr BP) shows little variation in the pollen record (Fig. 5). This zone is characterised by high percentages of *Azorella selago* (~70–80%) and a lower abundance of Poaceae (~10–20%), *Acaena magellanica* (0–3%) and *Carex austrocompacta* pollen (0–2%). *Botryococcus* and *Pediastrum* colonies abundance is low at on average 42% and 7% relative to the pollen sum, respectively. Pollen preservation is generally poorer than in sub-zone 1 and the damaged pollen grains are mostly corroded (Supplementary Fig. 6). LDT pollen influx is low (~10 grains $cm^{-2}yr^{-1}$) and shows a relatively high abundance of pollen from forest biome taxa like *Podocarpus* spp. (Fig. 5, Supplementary Fig. 6). Two single pollen grains of South American taxa *Nothofagus* and *Ephedra* were found (Fig. 5, Supplementary Fig. 6). Microcharcoal influx is relatively low (~30 grains $cm^{-2}yr^{-1}$).

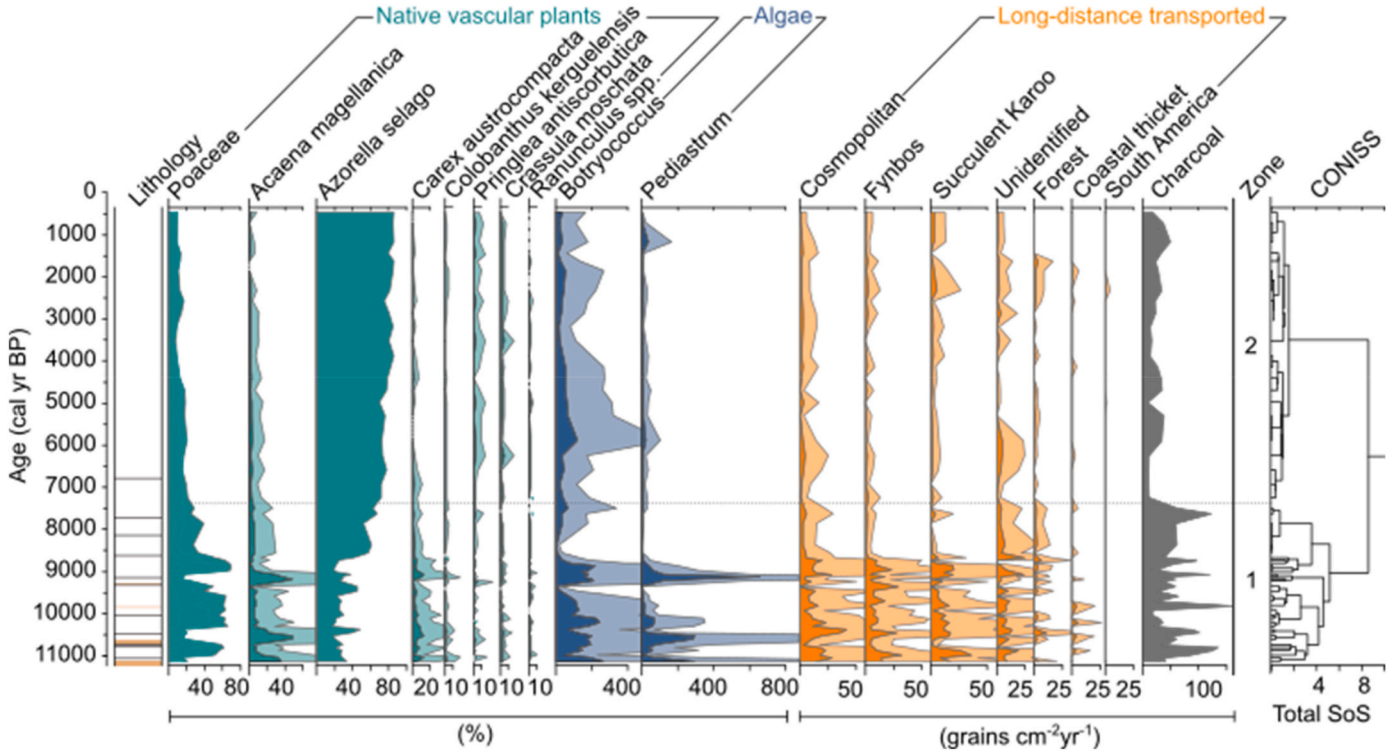

Fig. 5. Pollen diagram showing percentage data from the most common native taxa and influx values for long-distance transported (LDT) pollen and charcoal. The lighter shades depict 5x exaggeration to enhance readability. Zonation is based on the CONISS cluster dendrogram. SoS: Sum of Squares. Lithology according to Fig. 2.

4. Discussion

4.1. Lake 5 evolution

Based on the presented chronology (Fig. 4), infilling of the northern subbasin of Lake 5 (Fig. 1c) started around 11,300 cal yr BP, indicating deglaciation during the Early Holocene. This is in agreement with cosmogenic nuclide dating of glacial landforms on the southeast side of the Cook Ice Cap (Charton et al., 2022). The basal inorganic laminated sands (Fig. 2, lowermost beige layer) were likely deposited during deglaciation, when there was little vegetation to stabilize (glaciogenic) sediment in the catchment, and more powerful meltwater streams. Thereafter, sedimentation became more organic (Fig. 2), likely as a result of increased organic productivity and reduced minerogenic input through stabilization of the catchment (Kalugin et al., 2007). The inorganic laminated sand facies higher up in the core likely indicate increased sediment transport by higher runoff, possibly caused by increased precipitation or stronger meltwater streams.

The distinct laminations throughout the core argue for continuous sedimentation, interspersed by the coarse-grained event (E) layers (section 3.1 and 3.2). The geochemical signature of these event layers is characterised by positive values of elements from group 2 of the PCA: Zn, K, Zr, Rb, and Y (Fig. 3). This differs from the inorganic laminated sands at the base of the core which are associated with positive values of elements from group 1 of the PCA (Fig. 3), suggesting a different minerogenic source material. Elements from group 1 likely indicate weathering products of the basaltic bedrock (Gautier et al., 1990). The (coarse) sand and gravel characterized by high counts of elements from group 2 revealed the presence of tephra shards (Supplementary Fig. 4). PCA of XRF data from a peatbog on the eastern Kerguelen Islands revealed a similar grouping of elements (Zn, K, Zr, Rb, and Mn) compared to our group 2, this was interpreted to indicate volcanic ash (tephra) deposits (Van der Putten et al., 2015) related to volcanic activity from the southwestern Kerguelen Islands, which has a different geochemistry compared to the basaltic bedrock (Gagnevin et al., 2003; Gautier et al., 1990). Thick blankets of instantly deposited volcanic ash could drastically impact vegetation and runoff in the catchment (Yeloff et al., 2007), thereby overprinting the environmental signal captured by our proxies. However, considering the frequent reworking of ash deposits observed on the Kerguelen Islands (Van der Putten et al., 2015) and the erosive base of the event layers E1-E4, these layers might be reworked instead of primary material related to an eruption. Furthermore, our pollen record does not indicate significant changes following the thick event layers E1-E4 (Fig. 5). Considering the centennial-scale variability captured by the pollen record, this suggests that the deposition of these layers did not have long-term effects on the vegetation composition.

Our CT data reveal three intervals that contain folded and torn laminations (F layers in Supplementary Fig. 3, and section 3.1). Based on their visual correspondence with diagnostic soft sediment deformation structures as described by Oswald et al., (2021), they are attributed to seismically induced deformation. On the Kerguelen plateau, moderate (magnitude 5) earthquakes have occurred during historical times (Adams and Zhang, 1984). The CT imagery also shows that pebbles embedded in the fine-grained matrix leave an imprint in the layers below them (Supplementary Fig. 3), a characteristic of dropstones (Flisch and Becker, 2003). In high-latitude sites like Lake 5, these are typically transported over coring sites across seasonal lake ice cover (van der Bilt et al., 2018). As seen on Copernicus Sentinel-2 satellite imagery (EO Browser), Lake 5 is ice-covered during winter.

4.2. Holocene vegetation and climate history of the Kerguelen islands

4.2.1. Early Holocene warm period

In the Early Holocene, high percentages of pollen and spores from *Acaena magellanica*, *Carex austrocompacta*, *Lycopodium saururus*, and *Austroblechnum penna-marina* subsp. *penna-marina* – formerly named *Blechnum penna-marina* (De Gasper et al., 2016) – indicate a broad climate optimum. These species thrive in sheltered habitats under warm conditions (Young and Schofield, 1973). The relatively high abundance of the semi-aquatic *Ranunculus* spp. in the Early Holocene suggests relatively wet conditions (Fig. 5). The anti-phased variability between *Acaena magellanica* and Poaceae pollen abundance suggest variable local conditions. *Acaena magellanica* pollen peak after intervals of the inorganic laminated sand facies indicative of unstable conditions in the catchment after deglaciation and higher runoff into Lake 5 (Fig. 5). Due to its sturdy woody stems, *Acaena magellanica* is well adapted to establish itself on unstable substrates (Greene, 1964), while shallow rooting grasses are less resistant to reworking of sediment and increased weathering (Frenot et al., 1998). Furthermore, peaks in the abundance of freshwater green algae *Pediastrum* and *Botryococcus* coincide with peaks in *Acaena magellanica* pollen abundance. The algae indicate open water, warm/higher temperatures, and optimal nutrient and light conditions in the water column (Björck et al., 1993; Guy-Ohlson, 1992). The fluctuating algal abundance (Fig. 5) hints at changes in lake level and turbulence (Markgraf et al., 2003). Additionally, the preservation of pollen shows a relatively high percentage of crumpled pollen, suggesting mechanical deterioration during transportation (McCulloch et al., 2020). Based on this, we suggest that Early Holocene variability largely stems from local changes in catchment dynamics, possibly linked to changes in precipitation or meltwater causing increased surface runoff (Smith et al., 2001).

High inc/coh and co-varying LOI values in the organic laminated mud facies (Fig. 2), suggest high organic matter production in the Early Holocene in and around Lake 5. These indicators have shown a positive correlation with annual temperature (Kalugin et al., 2007). Moreover, relatively few drop stones were found in the sediment from 11,300 to 9,300 cal yr BP, indicating that lake ice coverage was less severe (Flisch and Becker, 2003).

Summarised, our data point to a warm and dynamic Early Holocene climate on the Kerguelen Islands. A warm Early Holocene is also inferred from palynological records on the eastern Kerguelen Islands (Van der Putten et al., 2015; Young and Schofield, 1973). Diatom-derived Sea surface temperature (SST) reconstructions from MD11-3353 south of the Kerguelen Islands (Fig. 1a), suggest that the Polar Front was located further south during the Early Holocene (Fig. 6i) (Civel-Mazens et al., 2021), allowing warmer subtropical water masses to reach the Kerguelen Islands. This is consistent with low sea-ice concentrations in the Indian sector of the Southern ocean (Fig. 6j) (Orme et al., 2020), and the well-established early Holocene Thermal Maximum that is also seen in temperature reconstructions from Antarctica (Stenni et al., 2010).

4.2.2. Mid-to Late Holocene cooling

Starting ~8,600 cal yr BP, the transition into the Mid Holocene is characterised by the rapid increase in *Azorella selago* pollen abundance and a decline in abundance of most other native taxa, except for *Pringlea antiscorbutica* (Fig. 5, Supplementary Fig. 6). *Azorella selago* and *Pringlea antiscorbutica* can grow on cold and relatively dry windswept ridges (Young and Schofield, 1973). Concurrently, we find an increase of corroded and degraded pollen grains in the Late Holocene (Supplementary Fig. 6). Pollen is best preserved in acidic and anaerobic conditions: corroded and degraded pollen are a sign of deterioration through oxidation or microbial activity under a drier aerobic environment (Mansilla et al., 2018; McCulloch et al., 2020). Therefore, we interpret the pollen record to show a general trend towards a colder and drier climate on the Kerguelen Islands. This is supported by the lower abundance of green algae, and a decline in productivity as seen by a lower organic matter content of the sediments (Figs. 2 and 5). Furthermore, there is a regular occurrence of drop stones in the sediment, indicating more frequent ice coverage on the lake from ~9,300 cal yr BP. A transition to colder climate conditions is consistent with a decline in SST south of the Kerguelen Islands (Civel-Mazens et al., 2021), an

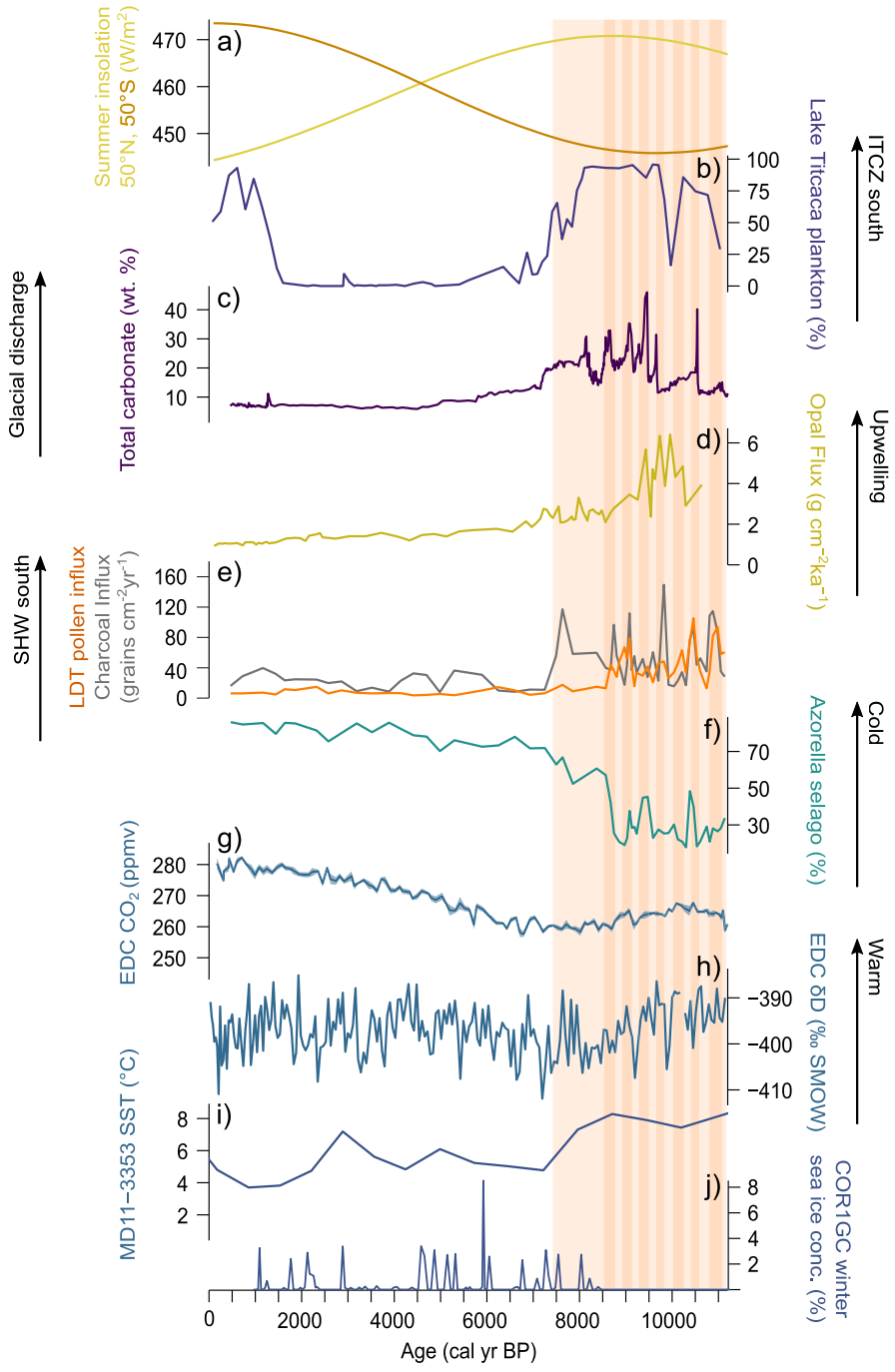

Fig. 6. Comparison between **a)** 50°N (JJA) and 50°S (DJF) summer insolation calculated using the Palinsol package in R (Crucifix, 2016), **b)** plankton (%) in Lake Titicaca, representative of shifts in the ITCZ (Baker et al., 2001), **c)** detrital carbonate peaks (total carbonate) from MD99-2236, representing glacial meltwater pulses in the Hudson strait, North Atlantic (Jennings et al., 2015), **d)** opal flux from site TN057-13, indicative for upwelling in the Southern Ocean (Anderson et al., 2009; Kaplan et al., 2016), **e)** data from this study: influx of LDT pollen and charcoal (grains $cm^{-2}yr^{-1}$), **f)** data from this study: *Azorella selago* pollen abundance (%), **g)** CO_2 (ppmv) record from EPICA Dome C (Monnin et al., 2004), **h)** δD (‰SMOW) record from EPICA Dome C (Stenni et al., 2010) on the updated AICC2012 chronology (Veres et al., 2013), **i)** Summer sea surface temperature (SST) record based on diatom assemblages from MD11-3353 south of the Kerguelen Islands (Civel-Mazens et al., 2021), **j)** winter mean sea-ice concentration record based on diatom assemblages from COR1GC in the Indian Ocean (Orme et al., 2020). Light orange shading indicates the inferred more southerly position of the SHW during the Early Holocene, and darker orange bars show peaks in LDT pollen from the Lake 5 record.

increase in sea-ice concentration in the Indian sector of the Southern Ocean (Fig. 6j) (Orme et al., 2020), and cooler temperatures in Antarctica (Jones et al., 2023; Stenni et al., 2010, Fig. 6).

From ~7,400 cal yr BP onwards, there is little variation in the pollen record (Fig. 5, zone 2), indicating that cold climate conditions prevailed over the Kerguelen Islands throughout the Mid-to Late Holocene. No other high-resolution palynological records exist for this period on the Kerguelen Islands (Roche-Bellair and Piveteau, 1976; Young and Schofield, 1973), but a Cook Ice Cap glacier reconstructions also show stable conditions in the Mid Holocene, until readvances after 2,000 cal yr BP (Charton et al., 2022). This contrasts with other palaeobotanical and palynological records within the zone of SHW influence that show

several climatic changes during this time interval (e.g. Moreno et al., 2018; Van der Putten et al., 2008; Zwier et al., 2022).

During the last 500 years, rising LOI and inc/coh values indicate an increase in organic productivity (Fig. 2) as a response to a slight warming as also seen from increased CO_2 and $d^{18}O$ values in the EPICA Dome C (EDC) ice core record (Monnin et al., 2004) (Fig. 6). However, pollen concentrations were too low in the top sediments to further substantiate these inferences.

4.3. Wind proxy interpretation

4.3.1. Provenance of LDT pollen

We use LDT pollen fluxes as indicators of regional wind fields. Most LDT pollen found in our Lake 5 record derive from southern Africa (Fig. 5, Supplementary Fig. 6), in agreement with forward trajectory models that show transport of microscopic particles from South Africa in a south-easterly direction towards the Kerguelen Islands (Neff and Bertler, 2015). In our record, peaks in total LDT pollen influx occurred in the Early Holocene when the native pollen indicate that relatively warm conditions prevailed on the Kerguelen Islands (Fig. 5, section 4.2.1). A reduced influx of LDT pollen after 8,600 cal yr BP coincided with a shift to colder conditions captured by native pollen during the Mid-to Late Holocene (Fig. 5, section 4.2.2). The coincidence of warmer local temperatures with a greater abundance of LDT pollen from the northeast (southern Africa) during the Early Holocene, is best explained by an average position of the SHW core belt to the south of the Kerguelen Islands, as this would bring warm sub-tropical ocean currents and air-masses and storm tracks containing pollen and charcoal from southern Africa to the islands (Civel-Mazens et al., 2021; Denton et al., 2021; Fogt and Marshall, 2020; Hahn et al., 2017; Spoth et al., 2023), similar to SAM positive-like conditions (Fogt and Marshall, 2020). Similarly, the coincidence of colder local temperatures with a reduction of southward-transported LDT pollen, is best explained by an average position of the SHW core belt further to the north of the Kerguelen Islands, as this brings cold polar airmasses from around Antarctica to the Kerguelen Islands, devoid of LDT pollen, akin to SAM negative-like conditions (Fogt and Marshall, 2020). A similar interpretation was made by Spoth et al. (2023) with respect to past moisture source-areas of precipitation on the Falkland Islands, which are located at a similar latitude (52°S) as the Kerguelen Islands. They inferred that a southern position of the SHW led to the influence of sub-tropical moisture sources arriving through storm tracks from north of the Falklands, and vice versa. Furthermore, local warm conditions on the Kerguelen Island are linked to increased SST in the area (section 4.2, Fig. 6f and i). Model runs show that warmer SST around the Kerguelen Islands are caused by a poleward shift of the SHW (Denton et al., 2021).

Factors that affect the production of LDT pollen in their source regions, also need to be considered. The southern African biomes that supply LDT pollen to the Kerguelen Islands have distinct geographical origins (Scott and Neumann, 2018). Species turnover and expansion of the different biomes are on larger scales mainly modulated by climatic changes (Davies et al., 2022). Due to the frequently cyclonic nature of the wind fields over southern Africa (Garstang et al., 1996), we assume that the pollen load captured in our record contains a mix of pollen from the different biomes. More research would be needed to get more details on this relationship. In the Lake 5 record, we observe a relative increase in pollen from forest and coastal thicket biomes, concurrent with a relative decline in pollen from fynbos taxa around 8,600 cal yr BP (Supplementary Fig. 6b), although this occurs in a period with relatively low LDT pollen influx, and percentage differences are relatively small. Several records along the south coast of southern Africa indicate local forest expansion around this time in response to increased precipitation (Kirsten et al., 2020; Quick et al., 2018). Forest taxa like Podocarpaceae also have a significantly higher pollen production than non-arboreal taxa (Runge et al., 2015), which might explain this change in our record. However, the interactions between the tropical easterlies and temperate westerlies provide a complex picture of moisture distribution and associated vegetation dynamics in the coastal regions and continental interior of southern Africa (Chase et al., 2015; Chevalier and Chase, 2015; Strobel et al., 2022). More work studying atmospheric circulation dynamics and aerial pollen load is needed to decipher how African vegetation changes are reflected in relative changes of LDT pollen from the different source regions recorded in Lake 5.

4.3.2. Microcharcoal transport

The influx of microcharcoal particles is positively correlated to the influx of LDT pollen grains into Lake 5 (section 3.3), suggesting a common source area for the two. Although the size (60–100 μm) of some of the charred particles and their associated atmospheric lifetime might insinuate local burning on the Kerguelen Islands, particles up to 80 μm are known to be transported over distances on continental to global scale (Clark, 1988). A high frequency and abundance of both natural and human-induced fires has occurred in southern Africa throughout the entire Holocene (Davies et al., 2022; Power et al., 2008), while no natural occurrence of fires on the Kerguelen Island is known in this same period. Local fires could possibly have been ignited by lightning or volcanic activity (Castilla-Beltrán et al., 2023) from the volcanic complexes in the southwest of the Kerguelen Islands (Gautier et al., 1990). However, the vegetation on the island provides relatively little fuel for burning and the oftentimes patchy vegetation cover could prevent fires from spreading over large areas. Therefore, we suggest that most microcharcoal particles in our record originate from transport by the SHW.

4.4. Holocene SHW dynamics

4.4.1. Dynamic Early Holocene SHW

The centennial scale variability in our LDT pollen and charcoal influx records suggest that the SHW were very dynamic over the Kerguelen Islands during the Early Holocene (Figs. 5 and 6). The peaks in LDT particle influx reveal transport of particles from southern Africa to the Kerguelen Islands and suggest intervals with a position of the SHW core belt over, or south of the Kerguelen Islands (section 4.3.1). We suggest that in the Early Holocene the average position of SHW in the Indian Ocean sector was south of the Kerguelen Islands, and that minor changes of the SHW and its storm tracks resulted in the centennial scale variations in the LDT pollen record.

Precipitation on the Kerguelen Islands has been associated with shifts in SAM; southward moving storm tracks during a positive SAM state bring precipitation to the Kerguelen Islands (Favier et al., 2016). Different precipitation regimes during the centennial-scale variability of the SHW could therefore explain the variability in local taxa (primarily Poaceae and *Acaena*) and varying runoff regimes as inferred from the minerogenic content of the sediment (section 4.1 and 4.2.1).

Combined with other paleoclimatic records, we provide a regional reconstruction of SHW position shifts during the Holocene. Along the northern margin of the SHW, a reduced Early Holocene Westerly influence is seen in the winter-rainfall zone (WRZ) of southern Africa that experienced a dry period (Quick et al., 2022, and references therein). Several other terrestrial records support the interpretation of a southward-placed SHW in the Early Holocene. In Patagonia, pollen records indicate a more positive SAM-like state – associated with stronger and more southerly SHW – with a similar centennial scale variability as our Lake 5 record (Moreno et al., 2018). On the Falkland Islands, fluctuations in plant wax isotopes suggest highly variable alternations between a northern and southern moisture source in the Early Holocene (Spoth et al., 2023), indicating southward and northward shifts in the SHW position, respectively. This could argue for a zonally symmetric SHW response. However, not all proxy records indicate centennial-scale fluctuations whilst the SHW has a southerly position during the Early Holocene (e.g. Lamy et al., 2010; Monteath et al., 2022). This apparent discrepancy could be due to a number of reasons, including 1) the

sensitivity of the type of archive and proxies used, 2) a sampling resolution that was too low to pick up centennial-scale shifts, and 3) the latitudinal distance of the study site to the SHW core belt might have been too great to capture minor variations of the core wind belt.

Models indicate that a southward position of the SHW drives an increase in upwelling around Antarctica (Denton et al., 2021). Indeed, Anderson et al. (2009) found an increase in Southern Ocean upwelling in the Early Holocene when we infer a southward displacement of SHW (Fig. 6d). In addition, during the Early Holocene, the EDC ice-core record reveals relatively high atmospheric CO_2 concentrations concurrent with peaks in LDT pollen to Lake 5 (Fig. 6g). The Lake 5 record from the Kerguelen Islands provides strong support for the suggested connection between a southern SHW position, increased upwelling, and increased CO_2 ventilation from the ocean to the atmosphere (Anderson et al., 2009; Gottschalk et al., 2020; Toggweiler et al., 2006).

4.4.2. Stable mid-to Late Holocene SHW

Beginning ~8,600 cal yr BP, the reduced influx of LDT pollen (Figs. 5 and 6) indicates a northward movement of the SHW core belt. A SHW core belt position north of the Kerguelen Islands, allowing greater incursion of cold polar air, can explain the abundance of locally derived *Azorella selago* and *Pringlea antiscorbutica* pollen (Fig. 5). We interpret the northward shift of SHW to be analogous to the present-day austral winter state of the SHW when the wind belt is located further north and cold polar air reaches more northerly latitudes (Lamy et al., 2010).

Along the southwest coast of Africa, a shift to a predominantly winter rainfall regime is recorded around 8,000 cal yr BP, associated with an increased influence of the SHW (Kirsten et al., 2020; Quick et al., 2018). Proxy records from other sub-Antarctic islands also support a northwards SHW shift (McGlone et al., 2010; Monteath et al., 2022; Saunders et al., 2018; Spoth et al., 2023). LDT pollen and dust records from the Falkland Islands indicate the SHW shifted north between 10,000 and 6,500 cal yr BP (Monteath et al., 2022). Saunders et al. (2018) infer increased windblown dust over Macquarie Island (54°S) from 9,200 cal yr BP onwards, indicating increasing wind strength over the island. As Macquarie Island is currently located towards the northern edge of the SHW core belt, this increase in wind strength could indicate a northward shift in the SHW core belt towards the island's position/latitude. Diverging land- and sea surface temperature records from Campbell Island (52°S) and surrounding marine sites are also attributed to a northwards SHW shift after 9,000 cal yr BP (McGlone et al., 2010). The contemporaneous changes among these records indicate a hemisphere-wide symmetric northwards shift of the SHW.

From 7,400 cal yr BP onwards, climatic conditions were comparatively stable over the Kerguelen Islands, arguing that the SHW remained north of the Kerguelen Islands, and that a local stable cold climate prevailed in the Mid-to Late Holocene. In the WRZ of southern Africa reduced precipitation, linked to a reduced SHW influence, is recorded from ~7,500 until ~2,000 cal yr BP (Kirsten et al., 2020; Zhao et al., 2016). This might indicate that the SHW remained north of the Kerguelen Islands but not far enough north to influence southern Africa, or that wind speeds along the northern SHW margin decreased. We note that a number of other pollen records capture variations in SHW strength during this time (e.g. Mayr et al., 2007; Moreno et al., 2018; Zwier et al., 2022). These records are all from the Atlantic section of the Southern Hemisphere and might reflect a transition to zonally asymmetric behaviour of the SHW (Landschützer et al., 2015). Increased zonal asymmetry in SHW starting around 5,000 cal yr BP – expressed by differences in the SHW position and strength in different sectors of the southern mid-latitudes – was suggested by Fletcher and Moreno (2012), and attributed to modern-day El Niño Southern Oscillation (ENSO)-like processes. Another possibility is that differences observed among the Atlantic sector records result from their meridional proximity to the northward-shifted SHW position, resulting in greater sensitivity to smaller-scale variability of the wind belt position during the Mid-to Late Holocene, while the Kerguelen Islands were too far south of the SHW to be influenced.

4.5. Potential driving mechanisms

The warm climate conditions on the Kerguelen Islands and the southward shift of the SHW during the Early Holocene are difficult to explain by orbital forcing alone as Southern Hemisphere summer insolation was stable and low at the time (Fig. 6a). Alternatively, it has been suggested that similar millennial scale SHW shifts are driven by interhemispheric (tele)connections via changes in meridional heat transport (Anderson et al., 2009; Broecker, 1998; Buizert et al., 2018; Chase et al., 2011; Lamy et al., 2010; Orme et al., 2020; Toggweiler et al., 2006; Yuan et al., 2018). Notably, short-term Northern Hemisphere cold events weaken the Atlantic meridional overturning circulation (AMOC), affecting the heat distribution in both hemispheres, and forcing the thermal equator - expressed by the Inter Tropical Convergence Zone (ITCZ) (Fig. 6b)- into the warmer Southern Hemisphere (Baker et al., 2005; Ng et al., 2018; Schneider et al., 2014; Teller et al., 2002; Toggweiler, 2009). Such shifts also drive the SHW further south (Fogt and Marshall, 2020; Lee et al., 2011; Mariani et al., 2017; Yuan et al., 2018). While the main Northern Hemisphere cold events recognized to impact the Southern Hemisphere after deglaciation are Heinrich Event 1 and the Younger Dryas (Anderson et al., 2009 and references therein), smaller scale events also occurred during the Early Holocene (Studer et al., 2018; Thornalley et al., 2013). Throughout this period, several freshwater discharge events from the melting Laurentide Ice Sheet cooled North Atlantic climate (Jennings et al., 2015). In keeping with the afore-mentioned mechanism to redistribute heat across both hemispheres, meltwater forcing could have pushed the SHW southwards during the Early Holocene. This notion is supported by the agreement between peaks in LDT particles (pollen and charcoal) in Lake 5 and meltwater discharge peaks (Fig, 6c and e). We should, however, note that the uncertainties of both age-depth models and the short duration of these event, hinder confident attribution.

Considering the on-going amplified warming of the Northern hemisphere, and the expected increase in freshwater fluxes from the melting of the Greenland ice sheet affecting meridional overturning circulation (Aguiar et al., 2021; Yuan et al., 2018 and references therein), this is especially important for understanding what might happen to major atmospheric and oceanic circulation patterns under future climate scenarios (King et al., 2023).

5. Conclusions

Native pollen and geochemical characteristics of the sediment revealed relative warm but variable climate conditions on the Kerguelen Islands in the Early Holocene, followed by a transition to colder, more stable conditions beginning 8,600 cal yr BP. The LDT pollen and microcharcoal records allowed us to reconstruct the timing and latitudinal position of SHW in the Indian Sector of the Southern Ocean. Based on changes in the influx of LDT pollen and microcharcoal from southern Africa to our field site on the Kerguelen Islands, we infer that the core belt of the SHW was on average located south of the Kerguelen Islands during the Ealy Holocene and shifted northward beginning 8,600 cal yr BP. These results place important latitudinal constraints on the timing of the SHW dynamics through a direct tracer of atmospheric circulation and support interpretations of an Early Holocene southwards displacement of the SHW proposed by other paleoclimate studies in the sub-Antarctic. We suggest that these changes might be driven by teleconnections to climate events in the Northern Hemisphere, but further work on the timing of events needs to be done to constrain these inferences. Our findings indicate that future studies on LDT pollen grains as tracers of atmospheric circulation on sub-Antarctic islands might help constrain the timing, latitudinal extent, and circumpolar symmetry of SHW shifts.

Author contributions

MZ contributed to Conceptualization, Investigation, Formal analysis, Visualization, and led the Manuscript writing – original draft, review & editing. WGMB contributed to Conceptualization, Funding acquisition, Investigation, Supervision, Writing – original draft, review & editing. TS contributed to Formal analysis, Writing – review & editing. WJDA contributed supervision, Writing – review & editing. JB contributed to Resources, Funding acquisition, Writing – review & editing. NVP contributed to Resources, Writing – review & editing. AEB contributed to Conceptualization, Funding acquisition, Supervision, Writing – original draft, review & editing.

Declaration of competing interest

The authors declare that they have no known competing financial interests or personal relationships that could have appeared to influence the work reported in this paper.

Data availability

Palynological data and the age-depth model will be made accessible in the Neotoma Paleoecology Database and sedimentological data will be accessible on Dataverse.no upon publication.

Acknowledgements

This research was supported by NFR grant project number 267719 (SOUTHSPHERE) and the Bjerknes Centre for Climate Research visiting fellow grant. Maaike Zwier's contribution was supported by a Meltzer project grant for students and PhD. Willem van der Bilt's contribution was supported by a Starting Grant (TMS2021STG01) from the Trond Mohn Stiftelse (TMS). Tobias Schneider was supported by the SNSF Postdoc. Mobility grant (P400P2_199323) and SNSF Return CH Postdoc. Mobility grant (P5R5PN_214300). We thank Eivind Støren and Aart Verhage for their help during the fieldwork. We are grateful to Henriette Linge for collecting modern plant samples in the field and discussion of results. Thanks to Jan Magne Cederstrøm, Talin Tuestad, Violeth Swai, and Andreea Auer for their help and discussions in the sediment laboratory and Ali Bolkar Kılıç who performed the MS scanning. We are grateful to Lynne Quick and Evi Naudts for their help with identification of African pollen species. Lastly, we would like to thank the two anonymous reviewers for their helpful contributions to improve this manuscript.

Appendix A. Supplementary data

Supplementary data to this article can be found online at https://doi.org/10.1016/j.quascirev.2024.108595.

References

Abram, N.J., Mulvaney, R., Vimeux, F., Phipps, S.J., Turner, J., England, M.H., 2014. Evolution of the southern annular mode during the past millennium. Nat. Clim. Change 4, 564–569. https://doi.org/10.1038/nclimate2235.

Adams, R.D., Zhang, B.M., 1984. A further earthquake on the Kerguelen Plateau. Geophys. J. Roy. Astron. Soc. 79, 697–703. https://doi.org/10.1111/j.1365-246X.1984.tb02248.x.

Aguiar, W., Meissner, K.J., Montenegro, A., Prado, L., Wainer, I., Carlson, A.E., Mata, M. M., 2021. Magnitude of the 8.2 ka event freshwater forcing based on stable isotope modelling and comparison to future Greenland melting. Sci. Rep. 11, 1–10. https://doi.org/10.1038/s41598-021-84709-5.

Anderson, R.F., Ali, S., Bradtmiller, L.I., Nielsen, S.H.H., Fleisher, M.Q., Anderson, B.E., Burckle, L.H., 2009. Wind-driven upwelling in the southern ocean and the deglacial rise in atmospheric CO2. Science 323, 1443–1448. https://doi.org/10.1126/science.1167441.

Arnaud, F., Magand, O., Chapron, E., Bertrand, S., Boës, X., Charlet, F., Mélières, M.A., 2006. Radionuclide dating (210Pb, 137Cs, 241Am) of recent lake sediments in a highly active geodynamic setting (Lakes Puyehue and Icalma-Chilean Lake District). Sci. Total Environ. 366, 837–850. https://doi.org/10.1016/j.scitotenv.2005.08.013.

Baker, P.A., Seltzer, G.O., Fritz, S.C., Dunbar, R.B., Grove, M.J., Tapia, P.M., Cross, S.L., Rowe, H.D., Broda, J.P., 2001. The history of South American tropical precipitation for the past 25,000 years, 80 Science 291, 640–643. https://doi.org/10.1126/science.291.5504.640.

Baker, P.A., Fritz, S.C., Garland, J., Ekdahl, E., 2005. Holocene hydrologic variation at Lake Titicaca, Bolivia/Peru, and its relationship to North Atlantic climate variation. J. Quat. Sci. 20, 655–662. https://doi.org/10.1002/jqs.987.

Barrow, C.J., 1976. Palynological studies in South Georgia: 1. Pollen and spore morphology of the native vascular species. Br. Antarct. Surv. Bull. 43, 67–73.

Bellair, N., 1970. Palynologie d'une tourbière de Pointe-Denis (péninsule Courbet, Kerguelen). Bull. l'Association française pour l'étude du Quat. 7, 49–51. https://doi.org/10.3406/quate.1970.1147.

Bishop, T., 2022. Using Itrax Data in R.

Björck, S., Håkansson, H., Olsson, S., Barnekow, L., Janssens, J., 1993. Palaeoclimatic studies in South Shetland Islands, Antarctica, based on numerous stratigraphic variables in lake sediments. J. Paleolimnol. 8, 233–272. https://doi.org/10.1007/BF00177858.

Blaauw, M., Christen, J.A., Lopez, M.A.A., Vazquez, J.E., O.M.G., V., Belding, T., Theiler, J., Gough, B., Karney, C., 2022. Age-Depth Modelling Using Bayesian Statistics.

Broecker, W.S., 1998. Paleocean circulation during the last deglaciation: a bipolar seesaw? Paleoceanography 13, 119–121. https://doi.org/10.1029/97PA03707.

Buizert, C., Sigl, M., Severi, M., Markle, B.R., Wettstein, J.J., McConnell, J.R., Pedro, J.B., Sodemann, H., Goto-Azuma, K., Kawamura, K., Fujita, S., Motoyama, H., Hirabayashi, M., Uemura, R., Stenni, B., Parrenin, F., He, F., Fudge, T.J., Steig, E.J., 2018. Abrupt ice-age shifts in southern westerly winds and Antarctic climate forced from the north. Nature 563, 681–685. https://doi.org/10.1038/s41586-018-0727-5.

Castilla-Beltrán, A., Monteath, A., Jensen, B.J.L., Nascimento, L. de, María Fernández-Palacios, J., Strandberg, N., Edwards, M., Nogué, S., 2023. Taming Fogo Island: late-Holocene volcanism, natural fires and land use as recorded in a scoria-cone sediment sequence in Cabo Verde. Holocene 33, 371–381. https://doi.org/10.1177/09596836221145442.

Charton, J., Schimmelpfennig, I., Jomelli, V., Delpech, G., Blard, P.H., Braucher, R., Verfaillie, D., Favier, V., Rinterknecht, V., Goosse, H., Crosta, X., Chassiot, L., Martin, L., Guillaume, D., Legentil, C., 2022. New cosmogenic nuclide constraints on late glacial and holocene glacier fluctuations in the sub-antarctic Indian ocean (kerguelen islands, 49°S). Quat. Sci. Rev. 283 https://doi.org/10.1016/j.quascirev.2022.107461.

Chase, B.M., Quick, L.J., Meadows, M.E., Scott, L., Thomas, D.S.G., Reimer, P.J., 2011. Late glacial interhemispheric climate dynamics revealed in South African hyrax middens. Geology 39, 19–22. https://doi.org/10.1130/G31129.1.

Chase, B.M., Lim, S., Chevalier, M., Boom, A., Carr, A.S., Meadows, M.E., Reimer, P.J., 2015. Influence of tropical easterlies in southern Africa's winter rainfall zone during the Holocene. Quat. Sci. Rev. 107, 138–148.

Chevalier, M., Chase, B.M., 2015. Southeast African records reveal a coherent shift from high- to low-latitude forcing mechanisms along the east African margin across last glacial-interglacial transition. Quat. Sci. Rev. 125, 117–130. https://doi.org/10.1016/j.quascirev.2015.07.009.

Chevalier, M., Chase, B.M., Quick, L.J., Scott, L., 2021. Atlas of Southern African Pollen Taxa (V1.1. https://doi.org/10.5281/zenodo.4013452 [WWW Document].

Civel-Mazens, M., Crosta, X., Cortese, G., Michel, E., Mazaud, A., Ther, O., Ikehara, M., Itaki, T., 2021. Impact of the agulhas Return current on the oceanography of the Kerguelen plateau region, Southern Ocean, over the last 40 kyrs. Quat. Sci. Rev. 251, 106711 https://doi.org/10.1016/j.quascirev.2020.106711.

Clark, J.S., 1988. Particle motion and the theory of charcoal analysis: source area, transport, deposition, and sampling. Quat. Res. 30, 67–80. https://doi.org/10.1016/0033-5894(88)90088-9.

Croudace, I.W., Rindby, A., Rothwell, R.G., 2006. ITRAX: description and evaluation of a new multi-function X-ray core scanner. Geol. Soc. Spec. Publ. 267, 51–63. https://doi.org/10.1144/GSL.SP.2006.267.01.04.

Crucifix, M., 2016. Palinsol: Insolation for Palaeoclimate Studies. R Package Version.

Davies, S.J., Lamb, H.F., Roberts, S.J., 2015. Micro-XRF Core Scanning in Palaeolimnology: Recent Developments. Springer, Dordrecht, pp. 189–226. https://doi.org/10.1007/978-94-017-9849-5_7.

Davies, B., Power, M.J., Braun, D.R., Douglass, M.J., Mosher, S.G., Quick, L.J., Esteban, I., Sealy, J., Parkington, J., Faith, J.T., 2022. Fire and human management of late Holocene ecosystems in southern Africa. Quat. Sci. Rev. 289, 107600 https://doi.org/10.1016/j.quascirev.2022.107600.

De Gasper, A.L., Dittrich, V.A.D.O., Smith, A.R., Salino, A., 2016. A classification for Blechnaceae (Polypodiales: Polypodiopsida): new genera, resurrected names, and combinations. Phytotaxa 275, 191–227. https://doi.org/10.11646/phytotaxa.275.3.1.

Denton, G.H., Putnam, A.E., Russell, J.L., Barrell, D.J.A., Schaefer, J.M., Kaplan, M.R., Strand, P.D., 2021. The Zealandia Switch: ice age climate shifts viewed from Southern Hemisphere moraines. Quat. Sci. Rev. 257, 106771 https://doi.org/10.1016/j.quascirev.2020.106771.

EO Browser, n.d. https://apps.sentinel-hub.com/eo-browser/[WWW Document]. Sinergise Ltd..

Faegri, K., Iversen, J., 1989. Textbook of Pollen Analysis, fourth ed. John Wiley &Sons, Chichester.

Favier, V., Verfaillie, D., Berthier, E., Menegoz, M., Jomelli, V., Kay, J.E., Ducret, L., Malbéteau, Y., Brunstein, D., Gallée, H., Park, Y.H., Rinterknecht, V., 2016. Atmospheric drying as the main driver of dramatic glacier wastage in the southern Indian Ocean. Nat. Sci. Reports 6, 1–12. https://doi.org/10.1038/srep32396.

Fletcher, M.S., Moreno, P.I., 2011. Zonally symmetric changes in the strength and position of the Southern Westerlies drove atmospheric CO2 variations over the past 14 k. y. Geology 39, 419–422. https://doi.org/10.1130/G31807.1.
Fletcher, M.S., Moreno, P.I., 2012. Have the Southern Westerlies changed in a zonally symmetric manner over the last 14,000 years? A hemisphere-wide take on a controversial problem. Quat. Int. 253, 32–46. https://doi.org/10.1016/j.quaint.2011.04.042.
Flisch, A., Becker, A., 2003. Industrial X-ray computed tomography studies of lake sediment drill cores. Geol. Soc. Spec. Publ. 215, 205–212. https://doi.org/10.1144/GSL.SP.2003.215.01.19.
Fogt, R.L., Marshall, G.J., 2020. The southern annular mode: variability, trends, and climate impacts across the southern hemisphere. Wiley Interdiscip Rev. Clim. Chang. 11. https://doi.org/10.1002/wcc.652.
Frenot, Y., Gloaguen, J.C., Van De Vijver, B., Beyens, L., 1997. Datation de quelques sediments tourbeux holocenes et oscillations glaciaires aux iles Kerguelen. Comptes Rendus l'Académie des Sci. 320, 567–573. https://doi.org/10.1016/S0764-4469(97)84712-9.
Frenot, Y., Gloaguen, J.C., Cannavacciuolo, M., Bellido, A., 1998. Primary succession on glacier forelands in the subantarctic Kerguelen Islands. J. Veg. Sci. 9, 75–84. https://doi.org/10.2307/3237225.
Frölicher, T.L., Sarmiento, J.L., Paynter, D.J., Dunne, J.P., Krasting, J.P., Winton, M., 2015. Dominance of the Southern Ocean in anthropogenic carbon and heat uptake in CMIP5 models. J. Clim. 28, 862–886. https://doi.org/10.1175/JCLI-D-14-00117.1.
Gagnevin, D., Ethien, R., Bonin, B., Moine, B., Féraud, G., Gerbe, M.C., Cottin, J.Y., Michon, G., Tourpin, S., Mamias, G., Perrache, C., Giret, A., 2003. Open-system processes in the genesis of silica-oversaturated alkaline rocks of the Rallier-du-Baty Peninsula, kerguelen Archipelago (Indian ocean). J. Volcanol. Geoth. Res. 123, 267–300. https://doi.org/10.1016/S0377-0273(02)00509-7.
Garstang, M., Tyson, P.D., Swap, R., Edwards, M., Kållberg, P., Lindesay, J.A., 1996. Horizontal and vertical transport of air over southern Africa. J. Geophys. Res. Atmos. 101, 23721–23736. https://doi.org/10.1029/95jd00844.
Gautier, I., Weis, D., Mennessier, J.P., Vidal, P., Giret, A., Loubet, M., 1990. Petrology and geochemistry of the Kerguelen Archipelago basalts (South Indian Ocean): evolution of the mantle sources from ridge to intraplate position. Earth Planet Sci. Lett. 100, 59–76. https://doi.org/10.1016/0012-821X(90)90176-X.
Goslar, T., Czernik, J., Goslar, E., 2004. Low-energy 14C AMS in Poznań radiocarbon laboratory, Poland. Nucl. Instruments Methods Phys. Res. Sect. B Beam Interact. with Mater. 5–11. https://doi.org/10.1016/j.nimb.2004.04.005. Atoms 223–224.
Gottschalk, J., Michel, E., Thöle, L.M., Studer, A.S., Hasenfratz, A.P., Schmid, N., Butzin, M., Mazaud, A., Martínez-García, A., Szidat, S., Jaccard, S.L., 2020. Glacial heterogeneity in Southern Ocean carbon storage abated by fast South Indian deglacial carbon release. Nat. Commun. 11, 1–14. https://doi.org/10.1038/s41467-020-20034-1.
Greene, S.W., 1964. The Vascular Flora of South Georgia. British Antarctic Survey Scientific Report No. 45. Britisch Antarctic Survey, London.
Greene, S.W., Greene, D.M., 1963. Check list of the sub-Antarctic and Antarctic vascular flora. Polar Rec. 11, 411–418. https://doi.org/10.1017/S0032247400053535.
Grimm, E.C., 1987. CONISS: a FORTRAN 77 program for stratigraphically constrained cluster analysis by the method of incremental sum of squares. Comput. Geosci. 13, 13–35. https://doi.org/10.1016/0098-3004(87)90022-7.
Grimm, E.C., 1992. Tilia and Tilia-Graph.
Guy-Ohlson, D., 1992. Botryococcus as an aid in the interpretation of palaeoenvironment and depositional processes. Rev. Palaeobot. Palynol. 71, 1–15. https://doi.org/10.1016/0034-6667(92)90155-A.
Hahn, A., Schefuß, E., Andò, S., Cawthra, H.C., Frenzel, P., Kugel, M., Meschner, S., Mollenhauer, G., Zabel, M., 2017. Southern Hemisphere anticyclonic circulation drives oceanic and climatic conditions in late Holocene southernmost Africa. Clim. Past 13, 649–665. https://doi.org/10.5194/cp-13-649-2017.
Hall, A., Visbeck, M., 2002. Synchronous variability in the Southern Hemisphere atmosphere, sea ice, and ocean resulting from the annular mode. J. Clim. 15, 3043–3057. https://doi.org/10.1175/1520-0442(2002)015<3043:SVITSH>2.0.CO,2.
Heiri, O., Lotter, A.F., Lemcke, G., 2001. Loss on ignition as a method for estimating organic and carbonate content in sediments : reproducibility and comparability of results. J. Paleolimnol. 25, 101–110.
Hersbach, H., Bell, B., Berrisford, P., Hirahara, S., Horányi, A., Muñoz-Sabater, J., Nicolas, J., Peubey, C., Radu, R., Schepers, D., Simmons, A., Soci, C., Abdalla, S., Abellan, X., Balsamo, G., Bechtold, P., Biavati, G., Bidlot, J., Bonavita, M., De Chiara, G., Dahlgren, P., Dee, D., Diamantakis, M., Dragani, R., Flemming, J., Forbes, R., Fuentes, M., Geer, A., Haimberger, L., Healy, S., Hogan, R.J., Hólm, E., Janisková, M., Keeley, S., Laloyaux, P., Lopez, P., Lupu, C., Radnoti, G., de Rosnay, P., Rozum, I., Vamborg, F., Villaume, S., Thépaut, J.N., 2020. The ERA5 global reanalysis. Q. J. R. Meteorol. Soc. 146, 1999–2049. https://doi.org/10.1002/qj.3803.
Hodgson, D.A., Sime, L.C., 2010. Palaeoclimate: southern westerlies and CO2. Nat. Geosci. 3, 666–667. https://doi.org/10.1038/ngeo970.
Hogg, A.G., Heaton, T.J., Hua, Q., Palmer, J.G., Turney, C.S.M., Southon, J., Bayliss, A., Blackwell, P.G., Boswijk, G., Bronk Ramsey, C., Pearson, C., Petchey, F., Reimer, P., Reimer, R., Wacker, L., 2020. SHCal20 southern hemisphere calibration, 0-55,000 Years cal BP. Radiocarbon 62, 759–778. https://doi.org/10.1017/RDC.2020.59.
Jennings, A., Andrews, J., Pearce, C., Wilson, L., Ólfasdóttir, S., 2015. Detrital carbonate peaks on the Labrador shelf, a 13-7ka template for freshwater forcing from the Hudson Strait outlet of the Laurentide Ice Sheet into the subpolar gyre. Quat. Sci. Rev. 107, 62–80. https://doi.org/10.1016/j.quascirev.2014.10.022.
Jessen, C.A., Solignac, S., Nørgaard-Pedersen, N., Mikkelsen, N., Kuijpers, A., Seidenkrantz, M.S., 2011. Exotic pollen as an indicator of variable atmospheric circulation over the Labrador Sea region during the mid to late Holocene. J. Quat. Sci. 26, 286–296. https://doi.org/10.1002/jqs.1453.
Jones, T.R., Cuffey, K.M., Roberts, W.H.G., Markle, B.R., Steig, E.J., Stevens, C.M., Valdes, P.J., Fudge, T.J., Sigl, M., Hughes, A.G., Morris, V., Vaughn, B.H., Garland, J., Vinther, B.M., Rozmiarek, K.S., Brashear, C.A., White, J.W.C., 2023. Seasonal temperatures in west Antarctica during the holocene. Nature 613, 292–297. https://doi.org/10.1038/s41586-022-05411-8.
Juggins, S., 2015. rioja: anlaysis of Quaternary science data. R Doc 1–58.
Kalugin, I., Daryin, A., Smolyaninova, L., Andreev, A., Diekmann, B., Khlystov, O., 2007. 800-yr-long records of annual air temperature and precipitation over southern Siberia inferred from Teletskoye Lake sediments. Quat. Res. 67, 400–410. https://doi.org/10.1016/j.yqres.2007.01.007.
Kaplan, M.R., Schaefer, J.M., Strelin, J.A., Denton, G.H., Anderson, R.F., Vandergoes, M. J., Finkel, R.C., Schwartz, R., Travis, S.G., Garcia, J.L., Martini, M.A., Nielsen, S.H. H., 2016. Patagonian and southern South Atlantic view of holocene climate. Quat. Sci. Rev. 141, 112–125. https://doi.org/10.1016/j.quascirev.2016.03.014.
Kilian, R., Lamy, F., 2012. A review of Glacial and Holocene paleoclimate records from southernmost Patagonia (49-55°S). Quat. Sci. Rev. 53, 1–23. https://doi.org/10.1016/j.quascirev.2012.07.017.
King, J., Anchukaitis, K.J., Allen, K., Vance, T., Hessl, A., 2023. Trends and variability in the southern annular mode over the common Era. Nat. Commun. 14, 1–14. https://doi.org/10.1038/s41467-023-37643-1.
Kirsten, K.L., Kasper, T., Cawthra, H.C., Strobel, P., Quick, L.J., Meadows, M.E., Haberzettl, T., 2020. Holocene variability in climate and oceanic conditions in the winter rainfall zone of South Africa—inferred from a high resolution diatom record from Verlorenvlei. J. Quat. Sci. 35, 572–581. https://doi.org/10.1002/jqs.3200.
Kohfeld, K.E., Graham, R.M., de Boer, A.M., Sime, L.C., Wolff, E.W., Le Quéré, C., Bopp, L., 2013. Southern hemisphere westerly wind changes during the last glacial maximum: Paleo-data synthesis. Quat. Sci. Rev. 68, 76–95. https://doi.org/10.1016/j.quascirev.2013.01.017.
Kotov, S., Paelike, H., 2018. QAnalySeries - a cross-platform time series tuning and analysis tool. In: AGU Fall Meeting Abstracts, pp. PP53D–1230.
Kylander, M.E., Lind, E.M., Wastegård, S., Löwemark, L., 2012. Recommendations for using XRF core scanning as a tool in tephrochronology. Holocene 22, 371–375. https://doi.org/10.1177/0959683611423688.
Lamy, F., Kilian, R., Arz, H.W., François, J.P., Kaiser, J., Prange, M., Steinke, T., 2010. Holocene changes in the position and intensity of the southern westerly wind belt. Nat. Geosci. 3, 695–699. https://doi.org/10.1038/ngeo959.
Landschützer, P., Gruber, N., Haumann, F.A., Rödenbeck, C., Bakker, D.C.E., Van Heuven, S., Hoppema, M., Metzl, N., Sweeney, C., Takahashi, T., Tilbrook, B., Wanninkhof, R., 2015. The reinvigoration of the Southern Ocean carbon sink. Science 349, 1221–1224. https://doi.org/10.1126/science.aab2620.
Lee, S.Y., Chiang, J.C.H., Matsumoto, K., Tokos, K.S., 2011. Southern Ocean wind response to North Atlantic cooling and the rise in atmospheric CO2: modeling perspective and paleoceanographic implications. Paleoceanography 26. https://doi.org/10.1029/2010PA002004.
Mansilla, C.A., McCulloch, R.D., Morello, F., 2018. The vulnerability of the Nothofagus forest-steppe ecotone to climate change: Palaeoecological evidence from Tierra del Fuego (~53°S). Palaeogeogr. Palaeoclimatol. Palaeoecol. 508, 59–70. https://doi.org/10.1016/j.palaeo.2018.07.014.
Mariani, M., Fletcher, M.S., Drysdale, R.N., Saunders, K.M., Heijnis, H., Jacobsen, G., Zawadzki, A., 2017. Coupling of the intertropical convergence zone and southern hemisphere mid-latitude climate during the early to mid-holocene. Geology 45, 1083–1086. https://doi.org/10.1130/G39705.1.
Markgraf, V., Bradbury, J.P., Schwalb, A., Burns, S.J., Stern, C., Ariztegui, D., Gilli, A., Anselmetti, F.S., Stine, S., Maidana, N., 2003. Holocene palaeoclimates of southern Patagonia: Limnological and environmental history of Lago Cardiel, Argentina. Holocene 13, 581–591. https://doi.org/10.1191/0959683603hl648rp.
Mayr, C., Wille, M., Haberzettl, T., Fey, M., Janssen, S., Lücke, A., Ohlendorf, C., Oliva, G., Schäbitz, F., Schleser, G.H., Zolitschka, B., 2007. Holocene variability of the southern hemisphere westerlies in Argentinean Patagonia (52°S). Quat. Sci. Rev. 26, 579–584. https://doi.org/10.1016/j.quascirev.2006.11.013.
McCulloch, R.D., Blaikie, J., Jacob, B., Mansilla, C.A., Morello, F., De Pol-Holz, R., San Román, M., Tisdall, E., Torres, J., 2020. Late glacial and Holocene climate variability, southernmost Patagonia. Quat. Sci. Rev. 229, 106131 https://doi.org/10.1016/j.quascirev.2019.106131.
McGlone, M.S., Turney, C.S.M., Wilmshurst, J.M., Renwick, J., Pahnke, K., 2010. Divergent trends in land and ocean temperature in the Southern Ocean over the past 18,000 years. Nat. Geosci. 3, 622–626. https://doi.org/10.1038/ngeo931.
Meteoblue, 2023. WWW Document. https://www.meteoblue.com/en/weather/historyclimate/climatemodelled/port-aux-français_french-southern-territories_1546102, 2.2.24.
Monnin, E., Steig, E.J., Siegenthaler, U., Kawamura, K., Schwander, J., Stauffer, B., Stocker, T.F., Morse, D.L., Barnola, J.M., Bellier, B., Raynaud, D., Fischer, H., 2004. Evidence for substantial accumulation rate variability in Antarctica during the Holocene, through synchronization of CO2 in the Taylor Dome, Dome C and DML ice cores. Earth Planet Sci. Lett. 224, 45–54. https://doi.org/10.1016/J.EPSL.2004.05.007.
Monteath, A., Hughes, P., Cooper, M., Groff, D., Scaife, R., Hodgson, D., 2022. Late glacial – holocene record of southern hemisphere westerly wind dynamics from the Falkland Islands, south Atlantic ocean. Geology 1–6. https://doi.org/10.1130/G49805.1/5600732/g49805.pdf.
Moreno, P.I., Francois, J.P., Moy, C.M., Villa-Martínez, R., 2010. Covariability of the southern westerlies and atmospheric CO2 during the holocene. Geology 38, 727–730. https://doi.org/10.1130/G30962.1.

Moreno, P.I., Vilanova, I., Villa-Martínez, R., Dunbar, R., Mucciarone, D.M., Kaplan, M., Garreaud, R.D., Rojas, M., Moy, C.M., De Pol-Holz, R., Lambert, F., 2018. Onset and evolution of southern annular mode-like changes at centennial timescale. Sci. Rep. 8.
Moreno, P.I., Henríquez, W.I., Pesce, O.H., Henríquez, C.A., Fletcher, M.S., Garreaud, R. D., Villa-Martínez, R.P., 2021. An early Holocene westerly minimum in the southern mid-latitudes. Quat. Sci. Rev. 251, 106730 https://doi.org/10.1016/j.quascirev.2020.106730.
Neff, P.D., Bertler, N.A.N., 2015. Trajectory modeling of modern dust transport to the Southern Ocean and Antarctica. J. Geophys. Res. Atmos. 120, 9303–9322. https://doi.org/10.1002/2015JD023304.
Nelson Mandela University, 2019. Pollen Reference Collection for the Cape Floristic Region [WWW Document]. URL. https://pollen.mandela.ac.za/.
Nesje, A., 1992. A piston corer for lacustrine and marine sediments. Arct. Alp. Res. 24, 257–259. https://doi.org/10.2307/1551667.
Ng, H.C., Robinson, L.F., McManus, J.F., Mohamed, K.J., Jacobel, A.W., Ivanovic, R.F., Gregoire, L.J., Chen, T., 2018. Coherent deglacial changes in western Atlantic Ocean circulation. Nat. Commun. 9, 1–10. https://doi.org/10.1038/s41467-018-05312-3.
Oksanen, A.J., Blanchet, F.G., Friendly, M., Kindt, R., Legendre, P., Mcglinn, D., Minchin, P.R., Hara, R.B.O., Simpson, G.L., Solymos, P., Stevens, M.H.H., Szoecs, E., 2020. vegan: Community Ecology Package.
Orme, L.C., Crosta, X., Miettinen, A., Divine, D.V., Husum, K., Isaksson, E., Wacker, L., Mohan, R., Ther, O., Ikehara, M., 2020. Sea surface temperature in the Indian sector of the Southern Ocean over the late glacial and holocene. Clim. Past 16, 1451–1467. https://doi.org/10.5194/cp-16-1451-2020.
Oswald, P., Strasser, M., Hammerl, C., Moernaut, J., 2021. Seismic control of large prehistoric rockslides in the Eastern Alps. Nat. Commun. 12, 1–8. https://doi.org/10.1038/s41467-021-21327-9.
Pendlebury, S., Barnes-Keoghan, I., 2007. Climate and climate change in the sub-Antarctic. Pap. Proc. R. Soc. Tasmania I 67–81. https://doi.org/10.26749/rstpp.141.1.67.
Perren, B.B., Hodgson, D.A., Roberts, S.J., Sime, L., Van Nieuwenhuyze, W., Verleyen, E., Vyverman, W., 2020. Southward migration of the Southern Hemisphere westerly winds corresponds with warming climate over centennial timescales. Commun. Earth Environ. 1 https://doi.org/10.1038/s43247-020-00059-6.
Power, M.J., Marlon, J., Ortiz, N., Bartlein, P.J., Harrison, S.P., Mayle, F.E., Ballouche, A., Bradshaw, R.H.W., Carcaillet, C., Cordova, C., Mooney, S., Moreno, P. I., Prentice, I.C., Thonicke, K., Tinner, W., Whitlock, C., Zhang, Y., Zhao, Y., Ali, A.A., Anderson, R.S., Beer, R., Behling, H., Briles, C., Brown, K.J., Brunelle, A., Bush, M., Camill, P., Chu, G.Q., Clark, J., Colombaroli, D., Connor, S., Daniau, A.L., Daniels, M., Dodson, J., Doughty, E., Edwards, M.E., Finsinger, W., Foster, D., Frechette, J., Gaillard, M.J., Gavin, D.G., Gobet, E., Haberle, S., Hallett, D.J., Higuera, P., Hope, G., Horn, S., Inoue, J., Kaltenrieder, P., Kennedy, L., Kong, Z.C., Larsen, C., Long, C.J., Lynch, J., Lynch, E.A., McGlone, M., Meeks, S., Mensing, S., Meyer, G., Minckley, T., Mohr, J., Nelson, D.M., New, J., Newnham, R., Noti, R., Oswald, W., Pierce, J., Richard, P.J.H., Rowe, C., Sanchez Goñi, M.F., Shuman, B.N., Takahara, H., Toney, J., Turney, C., Urrego-Sanchez, D.H., Umbanhowar, C., Vandergoes, M., Vanniere, B., Vescovi, E., Walsh, M., Wang, X., Williams, N., Wilmshurst, J., Zhang, J.H., 2008. Changes in fire regimes since the last glacial maximum: an assessment based on a global synthesis and analysis of charcoal data. Clim. Dyn. 30, 887–907. https://doi.org/10.1007/s00382-007-0334-x.
Purich, A., Cai, W., England, M.H., Cowan, T., 2016. Evidence for link between modelled trends in Antarctic sea ice and underestimated westerly wind changes. Nat. Commun. 71 7, 1–9. https://doi.org/10.1038/ncomms10409, 2016.
Quick, L.J., Meadows, M.E., Bateman, M.D., Kirsten, K.L., Mäusbacher, R., Haberzettl, T., Chase, B.M., 2016. Vegetation and climate dynamics during the last glacial period in the fynbos-afrotemperate forest ecotone, southern Cape, South Africa. Quat. Int. 404, 136–149. https://doi.org/10.1016/j.quaint.2015.08.027.
Quick, L.J., Chase, B.M., Wündsch, M., Kirsten, K.L., Chevalier, M., Mäusbacher, R., Meadows, M.E., Haberzettl, T., 2018. A high-resolution record of Holocene climate and vegetation dynamics from the southern Cape coast of South Africa: pollen and microcharcoal evidence from Eilandvlei. J. Quat. Sci. 33, 487–500. https://doi.org/10.1002/jqs.3028.
Quick, L.J., Chase, B.M., Carr, A.S., Chevalier, M., Grobler, B.A., Meadows, M.E., 2022. A 25,000 year record of climate and vegetation change from the southwestern Cape coast, South Africa. Quat. Res. (United States) 105, 82–99. https://doi.org/10.1017/qua.2021.31.
R Core Team, 2022. R: A Langueage and Environment for Statistical Computing.
Reijmer, C.H., Van den Broeke, M.R., Scheele, M.P., 2002. Air parcel trajectories and snowfall related to five deep drilling locations in Antarctica based on the ERA-15 dataset. J. Clim. 15, 1957–1968. https://doi.org/10.1175/1520-0442(2002)015<1957:APTASR>2.0.CO, 2.
Reille, Maurice, 1992. Pollen et spores d'Europe et d'Afrique du nord. Laboratoire de Botanique historique et Palynologie.
Reynhout, S.A., Sagredo, E.A., Kaplan, M.R., Aravena, J.C., Martini, M.A., Moreno, P.I., Rojas, M., Schwartz, R., Schaefer, J.M., 2019. Holocene glacier fluctuations in Patagonia are modulated by summer insolation intensity and paced by Southern Annular Mode-like variability. Quat. Sci. Rev. 220, 178–187. https://doi.org/10.1016/j.quascirev.2019.05.029.
Roche-Bellair, N., Piveteau, J., 1976. Palynologie - les variations climatiques de l'holocène supérieur des îles Kerguelen: d'après la coupe d'une tourbière de la plaine de Dante (côte méridionale). Comptes Rendus Acad. des Sci. Paris 282, 1257–1260.
Rodrigues, L.A.C., Mendonça, C.B.F., Licínio, M.V.V.J., Agostini, K., da, M., Alencar, A.S., Gonçalves-Esteves, V., Antonio Costa Rodrigues, L., Barbieri Ferreira Mendonça, C., Vinicius Vaughan Jennings Licínio, M., da Matta Agostini, K., Santos Alencar, A., Gonçalves-Esteves, V., 2023. Diversity of pollen grains transported from South America to the Antarctic Peninsula through atmospheric dispersal. Polar Biol. 1.
QuaternaryVegetation dynamics – the African pollen Database, Palaeoecology of Africa. In: Runge, J., Gosling, W.D., Lézine, A., Scott, L. (Eds.), 2015. International Yearbook of Landscape Evolution and Palaeoenvironments. CRC Press.
Sandgren, P., Snowball, I.F., 2002. Application of mineral magnetic Techniques to Paleolimnology. In: Tracking Environmental Change Using Lake Sediments. Springer, Dordrecht, pp. 217–237. https://doi.org/10.1007/0-306-47670-3_8.
Saunders, K.M., Hodgson, D.A., Mcmurtrie, S., Grosjean, M., 2015. A diatom-conductivity transfer function for reconstructing past changes in the Southern Hemisphere westerly winds over the Southern Ocean. J. Quat. Sci. 30, 464–477. https://doi.org/10.1002/jqs.2788.
Saunders, K.M., Roberts, S.J., Perren, B., Butz, C., Sime, L., Davies, S., Van Nieuwenhuyze, W., Grosjean, M., Hodgson, D.A., 2018. Holocene dynamics of the Southern Hemisphere westerly winds and possible links to CO2 outgassing. Nat. Geosci. 11, 650–655. https://doi.org/10.1038/s41561-018-0186-5.
Schneider, T., Bischoff, T., Haug, G.H., 2014. Migrations and dynamics of the intertropical convergence zone. Nature 513, 45–53. https://doi.org/10.1038/nature13636.
Scott, L., 1982. Late quaternary fossil pollen grains from the Transvaal, South Africa. Rev. Palaeobot. Palynol. 36, 241–278. https://doi.org/10.1016/0034-6667(82)90022-7.
Scott, L., Neumann, F.H., 2018. Pollen-interpreted palaeoenvironments associated with the middle and late pleistocene peopling of southern Africa. Quat. Int. 495, 169–184. https://doi.org/10.1016/j.quaint.2018.02.036.
Smith, V.R., Steenkamp, M., Gremmen, N.J.M., 2001. Classification of the terrestrial habitats on Marion Island based on vegetation and soil chemistry. J. Veg. Sci. 12, 181–198. https://doi.org/10.2307/3236603.
Spoth, M., Hall, B., Lowell, T., Diefendorf, A.F., Corcoran, M.C., Brickle, P., Zhao, Y., 2023. Tracking the southern hemisphere westerlies during and since the last glacial maximum with multiproxy lake records from the Falkland Islands (52 S). Quat. Sci. Rev. 311 https://doi.org/10.1016/j.quascirev.2023.108135.
Stenni, B., Masson-delmotte, V., Selmo, E., Oerter, H., Meyer, H., Röthlisberger, R., Jouzel, J., Cattani, O., Falourd, S., Fischer, H., Hoffmann, G., Iacumin, P., Johnsen, S. J., Minster, B., Udisti, R., 2010. The deuterium excess records of EPICA Dome C and Dronning Maud Land ice cores (East Antarctica). Quat. Sci. Rev. 29, 146–159. https://doi.org/10.1016/j.quascirev.2009.10.009.
Strobel, P., Bliedtner, M., Carr, A.S., Struck, J., du Plessis, N., Glaser, B., Meadows, M.E., Quick, L.J., Zech, M., Zech, R., Haberzettl, T., 2022. Reconstructing Late Quaternary precipitation and its source on the southern Cape coast of South Africa: a multi-proxy paleoenvironmental record from Vankervelsvlei. Quat. Sci. Rev. 284 https://doi.org/10.1016/j.quascirev.2022.107467.
Strother, S.L., Salzmann, U., Roberts, S.J., Hodgson, D.A., Woodward, J., Van Nieuwenhuyze, W., Verleyen, E., Vyverman, W., Moreton, S.G., 2015. Changes in Holocene climate and the intensity of Southern Hemisphere Westerly Winds based on a high-resolution palynological record from sub-Antarctic South Georgia. Holocene 25, 263–279. https://doi.org/10.1177/0959683614557576.
Studer, A.S., Sigman, D.M., Martínez-García, A., Thöle, L.M., Michel, E., Jaccard, S.L., Lippold, J.A., Mazaud, A., Wang, X.T., Robinson, L.F., Adkins, J.F., Haug, G.H., 2018. Increased nutrient supply to the Southern Ocean during the Holocene and its implications for the pre-industrial atmospheric CO2 rise. Nat. Geosci. 11, 756–760. https://doi.org/10.1038/s41561-018-0191-8.
Swart, N.C., Fyfe, J.C., 2012. Observed and simulated changes in the Southern Hemisphere surface westerly wind-stress. Geophys. Res. Lett. 39 https://doi.org/10.1029/2012GL052810.
Teller, J.T., Leverington, D.W., Mann, J.D., 2002. Freshwater outbursts to the oceans from glacial Lake Agassiz and their role in climate change during the last deglaciation. Quat. Sci. Rev. 21, 879–887. https://doi.org/10.1016/S0277-3791(01)00145-7.
The Core Writing Team, Lee, H., Romer, J., 2023. Climate Change 2023: Synthesis Report. Contribution of Working Groups I, II and III to the Sixth Assessment Report of the Intergovernmental Panel on Climate Change. IPCC, Geneva, Switserland. https://doi.org/10.59327/IPCC/AR6-9789291691647.
Thompson, D.W.J., Wallace, J.M., 2000. Annular modes in the extratropical circulation. Part II: trends. J. Clim. 13, 1018–1036. https://doi.org/10.1175/1520-0442(2000)013<1018:AMITEC>2.0.CO, 2.
Thornalley, D.J.R., Blaschek, M., Davies, F.J., Praetorius, S., Oppo, D.W., McManus, J.F., Hall, I.R., Kleiven, H., Renssen, H., McCave, I.N., 2013. Long-term variations in Iceland-scotland overflow strength during the holocene. Clim. Past 9, 2073–2084. https://doi.org/10.5194/cp-9-2073-2013.
Toggweiler, J.R., 2009. Shifting westerlies. Science 323, 1434–1435.
Toggweiler, J.R., Russell, J.L., Carson, S.R., 2006. Midlatitude westerlies, atmospheric CO2, and climate change during the ice ages. Paleoceanography 21, 2005. https://doi.org/10.1029/2005PA001154.
Trouet, V., Van Oldenborgh, G.J., 2013. KNMI climate explorer: a web-based research tool for high-resolution paleoclimatology. Tree-Ring Res. 69, 3–13. https://doi.org/10.3959/1536-1098-69.1.3.
Turney, C.S.M., Jones, R.T., Fogwill, C.J., Hatton, J., Williams, A.N., Hogg, A., Thomas, Z.A., Palmer, J., Mooney, S., Reimer, R.W., 2016. A 250-year periodicity in Southern Hemisphere westerly winds over the last 2600 years. Clim. Past. https://doi.org/10.5194/cp-12-189-2016.
van der Bilt, W.G.M., Rea, B., Spagnolo, M., Roerdink, D.L., Jørgensen, S.L., Bakke, J., 2018. Novel sedimentological fingerprints link shifting depositional processes to Holocene climate transitions in East Greenland. Global Planet. Change 164, 52–64. https://doi.org/10.1016/j.gloplacha.2018.03.007.
van der Bilt, W.G.M., D'Andrea, W.J., Oppedal, L.T., Bakke, J., Bjune, A.E., Zwier, M., 2022. Stable Southern Hemisphere westerly winds throughout the Holocene until

intensification in the last two millennia. Commun. Earth Environ 3, 1–13. https://doi.org/10.1038/s43247-022-00512-8.

Van der Putten, N., Hébrard, J.P., Verbruggen, C., Van de Vijver, B., Disnar, J.R., Spassov, S., de Beaulieu, J.L., De Dapper, M., Keravis, D., Hus, J., Thouveny, N., Frenot, Y., 2008. An integrated palaeoenvironmental investigation of a 6200 year old peat sequence from Ile de la Possession, Iles Crozet, sub-Antarctica. Palaeogeogr. Palaeoclimatol. Palaeoecol. 270, 179–195. https://doi.org/10.1016/j.palaeo.2008.09.014.

Van der Putten, N., Verbruggen, C., Björck, S., Michel, E., Disnar, J.R., Chapron, E., Moine, B.N., de Beaulieu, J.L., 2015. The last termination in the South Indian ocean: a unique terrestrial record from kerguelen islands (49°S) situated within the Southern hemisphere westerly belt. Quat. Sci. Rev. 122, 142–157. https://doi.org/10.1016/j.quascirev.2015.05.010.

Van Zinderen Bakker, E.M., 1956a. South African Pollen Grains and Spores Part I. Amsterdam/Cape Town.

Van Zinderen Bakker, E.M., 1956b. South African Pollen Grains and Spores Part II. Amsterdam/Cape Town.

Van Zinderen Bakker, E.M., Coetzee, J.A., 1959. South African Pollen Grains and Spores Part III. Amsterdam/Cape Town.

Veres, D., Bazin, L., Landais, A., Toyé Mahamadou Kele, H., Lemieux-Dudon, B., Parrenin, F., Martinerie, P., Blayo, E., Blunier, T., Capron, E., Chappellaz, J., Rasmussen, S.O., Severi, M., Svensson, A., Vinther, B., Wolff, E.W., 2013. The Antarctic ice core chronology (AICC2012): an optimized multi-parameter and multi-site dating approach for the last 120 thousand years. Clim. Past 9, 1733–1748. https://doi.org/10.5194/cp-9-1733-2013.

Verfaillie, D., Charton, J., Schimmelpfennig, I., Stroebele, Z., Jomelli, V., Bétard, F., Favier, V., Cavero, J., Berthier, E., Goosse, H., Rinterknecht, V., Legentil, C., Charrassin, R., Aumaître, G., Bourlès, D.L., Keddadouche, K., 2021. Evolution of the Cook Ice Cap (Kerguelen Islands) between the last centuries and 2100 ce based on cosmogenic dating and glacio-climatic modelling. Antarct. Sci. 1–17. https://doi.org/10.1017/S0954102021000080.

Waterway, M.J., Wilson, K.L., Ford, B.A., Starr, J.R., Jin, X.F., Zhang, S.R., Gebauer, S., Hoffmann, M.H., Gehrke, B., Yano, O., Hoshino, T., Masaki, T., Ford, K.A., Chung, K. S., Jung, J., Kim, S., Escudero, M., Luceño, M., M, E., Martín-Bravo, S., Míguez, M., Villaverde, T., Molina, A., Simpson, D.A., Bruederle, L.P., Hahn, M., Hipp, A.L., Rothrock, P.E., Reznicek, A.A., Naczi, R.F.C., Thomas, W.W., Jiménez-Mejías, P., Roalson, E.H., Alverson, W.S., Cochrane, T.S., Spalink, D., Bruhl, J.J., 2015. Making Carex monophyletic (Cyperaceae, tribe Cariceae): a new broader circumscription. Bot. J. Linn. Soc. 179, 1–42. https://doi.org/10.1111/boj.12298.

Yeloff, D., Mauquoy, D., Barber, K., Way, S., Van Geel, B., Turney, C.S.M., 2007. Volcanic ash deposition and long-term vegetation change on subantarctic Marion Island. Arctic, Antarct. Alp. Res. 39, 500–511. https://doi.org/10.1657/1523-0430(06-040[YELOFF]2.0.CO;2.

Yin, J.H., 2005. A consistent poleward shift of the storm tracks in simulations of 21st century climate. Geophys. Res. Lett. 32, 1–4. https://doi.org/10.1029/2005GL023684.

Yost, C.L., Jackson, L.J., Stone, J.R., Cohen, A.S., 2018. Subdecadal phytolith and charcoal records from Lake Malawi, East Africa imply minimal effects on human evolution from the ~74 ka Toba supereruption. J. Hum. Evol. 116, 75–94. https://doi.org/10.1016/j.jhevol.2017.11.005.

Young, S.B., Schofield, E.K., 1973. Pollen evidence for late quaternary climate changes on Kerguelen Islands. Nature 245, 311–312. https://doi.org/10.1038/245311a0.

Yuan, X., Kaplan, M.R., Cane, M.A., 2018. The interconnected global climate system-a review of tropical-polar teleconnections. J. Clim. https://doi.org/10.1175/JCLI-D-16-0637.1.

Zhao, X., Dupont, L., Schefuß, E., Meadows, M.E., Hahn, A., Wefer, G., 2016. Holocene vegetation and climate variability in the winter and summer rainfall zones of South Africa. Holocene 26, 843–857. https://doi.org/10.1177/0959683615622544.

Zwier, M., van der Bilt, W.G., de Stigter, H., Bjune, A.E., 2022. Pollen evidence of variations in holocene climate and southern hemisphere westerly wind strength on sub-Antarctic south Georgia. Holocene 32, 147–158. https://doi.org/10.1177/09596836211060495.